

A Study of MHD and Monte Carlo
Simulations
of High-Current Plasma Beams in
Industrial Applications

by

Luping Zhang

A Thesis Submitted in Partial Fulfillment
of the Requirements for the Degree of
Master of Applied Science

in

The Faculty of Engineering and Applied Science

Mechanical Engineering

University of Ontario Institute of Technology

December 2015

© Luping Zhang, 2015

Abstract

In recent years, high-current plasma beams have been widely applied in industrial applications. Computational approaches help us easily understand plasma properties. In this thesis, the high-current plasma beams are simulated using Magnetohydrodynamics (MHD), Monte Carlo (MC), and Integrated Hybrid MHD and MC (IMHDMC) methods. For the new MHD method, the pressure, velocity and density of the high-current plasma beams are obtained by solving the mass, energy and momentum conservation equations, together with Ohm's law, Faraday's law and Ampere's law. For the new MC method, the MC algorithm and codes are developed to calculate the electron flux, heat and deposit energy based on the particle transport processes and collisions in magnetic fields. For the IMHDMC method, the density profiles of electron and argon ions are calculated in the MC modelling part and the temperature and Lorentz force are calculated in the MHD modelling part. The MHD, MC and IMHDMC methods are quantitatively and qualitatively verified by comparing the simulation results of the three methods with the real experiment data. The comparison and discussion between the MHD, MC and IMHDMC methods are presented from the theoretical and simulation aspects in detail.

The two specific cases have been briefly discussed: plasma gasification and fusion energy generation. This thesis is focused on developing new computational methods for high-current plasma beams to provide design and implementation references in industrial applications. The computational simulations help us understand the complex phenomena surrounding the high-current plasma beams and lead to better understanding of plasma dynamics involved in industrial applications.

Keywords: Plasma Beams Simulation, Magnetohydrodynamics(MHD) Method, ANSYS FLUENT, Monte Carlo (MC) Method, PHITS, Integrated Hybrid MHD and MC (IMHDMC) Method

Acknowledgements

I would like to express my sincere appreciation to my supervisor, Dr. Hossam A. Gabbar, Professor, Faculty of Energy Systems and Nuclear Science and Faculty of Engineering and Applied Science (FEAS) (cross faculty appointed), University of Ontario Institute of Technology (UOIT), for his continued assistance and guidance throughout this project.

I also would like to express my greatest gratitude to my colleagues in the Energy Safety and Control Laboratory (ESCL) at UOIT, for their inspiration and collaboration. Also, I would like to thank Dr. Barry Stoute for his support, and Eric Heritage for his contribution of Particle and Heavy Ion Transport code System (PHITS) software. I am grateful to all the staff in FEAS for providing me with all the necessary supports to finish this research.

Table of Contents

Abstract	i
Acknowledgements	ii
Table of Contents	iii
List of Figures	v
List of Tables	vii
1 Chapter 1: Introduction	1
1.1 Basic Plasma Physics	1
1.1.1 Definition of Plasma	1
1.1.2 Application of Plasma Physics.....	2
1.2 Plasma Modelling Methods.....	3
1.3 Motivation	3
1.4 Problem Definition.....	4
1.5 Objectives.....	5
1.6 Innovation / Contribution	8
1.7 Thesis Outline	9
2 Chapter 2: Literature Review	10
2.1 Theoretical Descriptions of Plasma Phenomena.....	10
2.1.1 Self-Consistent Formulation	11
2.1.2 Theoretical Approaches for Plasma Simulation.....	12
2.2 MHD Modelling for Plasmas	13
2.2.1 MHD Conservation Equations.....	13
2.2.2 Examples for 3D MHD Modelling	14
2.3 MC Modelling for Plasmas	16
2.3.1 Examples for MC Modelling	16
2.4 Hybrid Modelling for Plasmas	17
2.4.1 Examples for Hybrid Methods.....	18
2.5 Plasma Diagnostic Technology	19
3 Chapter 3: Methodology	20
3.1 Methodology for High-Current Plasma Beams.....	20
3.1.1 Flowchart for MHD Method.....	21
3.1.2 Flowchart for MC Method.....	21
3.1.3 Flowchart for IMHDMC Method	22
3.2 MHD Numerical Modelling	23
3.2.1 Assumptions	23
3.2.2 Governing Equations	24
3.2.3 Boundary Conditions	25
3.2.4 Thermodynamic Properties and Transport Coefficients	26
3.3 MC Numerical Modelling	27

3.3.1	MC Algorithm.....	28
3.3.2	Detailed MC Model	29
3.4	IMHDMC Numerical Modelling	32
3.4.1	Species and Models in IMHDMC Method	32
3.4.2	IMHDMC Algorithm	33
4	Chapter 4: High-Current Plasma Beams Simulation and Verification	36
4.1	MHD Simulation Results	36
4.1.1	Simulation Parameters	36
4.1.2	MHD Simulations	41
4.2	MC Simulation Results	45
4.2.1	Simulation Instruments	45
4.2.2	MC Simulation Steps	47
4.2.3	MC Simulations	49
4.3	IMHDMC Simulation Results.....	55
4.4	Experimental Verification	57
4.4.1	Current-Voltage Relation	57
4.4.2	High-Current Plasma Beam Experiment.....	58
4.4.3	Experimental Results and Analysis.....	60
4.4.3.3	One-Way Analysis of Variance	62
4.4.4	Three Methods Verification	63
5	Chapter 5: Comparison, Analysis and Discussion	66
5.1	Comparison and Analysis.....	66
5.2	Discussion	67
5.2.1	Theoretical Aspect	67
5.2.2	Simulation Aspect.....	68
6	Chapter 6: Conclusion and Future Work.....	69
6.1	Conclusion	69
6.2	Potential Applications	69
6.2.1	Fusion Energy Generation Application.....	69
6.2.2	Plasma Gasification Application.....	71
6.3	Future Work.....	72
	Appendices.....	74
	Appendix A: List of Acronyms	74
	Appendix B: Nomenclature.....	75
	Appendix C: Physical Constants.....	77
	References.....	79

List of Figures

Figure 1-1: Range of Temperature and Density of Plasmas; (b) Lighting over Las Cruces, New Mexico.	2
Figure 1-2: Principle of MHD Generator.....	3
Figure 2-1: Overall Theoretical Descriptions of Plasma Simulations	10
Figure 2-2: Langmuir Electrostatic Probe	19
Figure 3-1: MHD Flowchart by ANSYS FLUENT and Gambit for High-current Plasma beam	21
Figure 3-2: MC Flowchart by PHITS for High-Current Plasma Beam.....	22
Figure 3-3: IMHDMC Flowchart for High-Current Plasma Beam	22
Figure 3-4: MHD Model for High-Current Plasma Beam	23
Figure 3-5: Geometry of High-Current Plasma Beam	25
Figure 3-6: (a) Viscosity, (b) Thermal Conductivity and (c) Electrical Conductivity for Argon Gas	27
Figure 3-7: NEC of Argon Plasmas Calculated in Reference (—), in Reference ¹ (•) and Measured in Reference.....	27
Figure 3-8: MC Algorithm Permitting Simulation of Primary Electron Trajectories and Secondary Cascade Process in MC Model.....	28
Figure 3-9: Tally’s Definition and Functions in PHITS	29
Figure 3-10: MC Model for High-Current Plasma Beam.....	30
Figure 3-11: Cross Sections for Elastic Process (Ar^+/Ar), Excitation and Ionization (e^- and Ar) Processes in Phelps Database.....	33
Figure 3-12: Basic Plasma Processes in IMHDMC Model.....	34
Figure 4-1: Mesh Grids by Gambit for High-current Plasma Beam	37
Figure 4-2: Mesh Examination by Range Option and EquiAngle Skew Quality Type	38
Figure 4-3: 3D Mesh Examination by Sphere Option Display Type and EquiAngle Skew Quality Type.....	38
Figure 4-4: Overview of Pressure-based Algorithms	39
Figure 4-5: Second-order Upwind Scheme	40
Figure 4-6: Convergence History of High-current Plasma Beam	42
Figure 4-7: Static Pressure Distribution of Outlet in Radial Direction	42
Figure 4-8: Mass Weighted Average for Velocity at Outlet.....	43
Figure 4-9: Velocity Magnitude of Outlet in Radial Direction.....	44
Figure 4-10: 3D Density Distribution of High-Current Plasma Beam	44
Figure 4-11: 3D Velocity Vector of High-Current Plasma Beam	45
Figure 4-12: Notepad++ Programming Interface	46
Figure 4-13: Particle Transport Processes and Collisions in PHITS	46
Figure 4-14: Flowchart of MC Simulation.....	47

Figure 4-15: 3D MC Model by Tally [t-3dshow]	49
Figure 4-16: 2D MC Model by Tally [t-gshow] on (a) XY Plane and (b) XZ Plane.....	49
Figure 4-17: (a) Amount of Particles by Tally [t-product] and (b) The Relative Errors.....	50
Figure 4-18: (a) Electron Flux by Tally [t-track] on XY plane and (b) The Relative Errors..	52
Figure 4-19: (a) Electron Flux by Tally [t-track] on XZ Plane and (b) The Relative Errors..	53
Figure 4-20: Deposit Energy by Tally [t-deposit] in Cell 100.....	54
Figure 4-21: (a) Dose of Neutrons and Photons by Tally [t-heat] and (b) The Relative Errors	55
Figure 4-22: 1D Density Profiles of (a) e^- and (b) Ar^+ in IMHDMC Model.....	56
Figure 4-23: Validation of IMHDMC Method by References.....	56
Figure 4-24: (a) Temperature Distribution and (b) The Lorentz force in IMHDMC Model..	57
Figure 4-25: HOPE's Test Setup	59
Figure 4-26: High-current Plasma Beams Formed across Two Plasma Jets	59
Figure 4-27: (a) Current (Red Line) & Voltage (Blue Line) vs. Time and (b) Polynomial Equation for Voltage vs. Current in HOPE's Experiment	61
Figure 4-28: Power vs. Temperature in HOPE's Experiment.....	62
Figure 4-29: HOPE's Experiment (blue line), MHD Simulation (red line) and MC Simulation (black line) for Plasma Energy.....	64
Figure 6-1: Basic Z-pinch Mechanism.....	70
Figure 6-2: Four Intersecting Plasma Beam Model	70
Figure 6-3: Westinghouse Plasma Gasification. (Westinghouse Plasma Corporation).	71
Figure 6-4: Waste Processing by Plasma Gasification	72

List of Tables

Table 2-1: Three Main Approaches for Plasma Simulations	13
Table 2-2: MHD Equations.....	14
Table 3-1: Boundary Conditions for MHD Model	26
Table 3-2: Electron Motion Equations in MC Model.....	31
Table 3-3: Type of Species and Models in IMHDMC Method.....	33
Table 4-1: Overall Relationship between Q_{EAS} and Element Quality.....	37
Table 4-2: Physical Argon Properties in MHD Simulation	41
Table 4-3: Assisted Tools in MC Simulations	47
Table 4-4: Argon Gas and Copper Properties in MC Simulations.....	48
Table 4-5: Initial Conditions under Steady State in HOPE's Experiment	59
Table 4-6: Analysis of Variance (ANOVA) Table for Voltage	63
Table 4-7: ANOVA Table for Current.....	63
Table 5-1: Similarities and Differences between MHD and MC Simulations.....	67
Table 5-2: Comparison between MHD, MC and IMHDMC Methods	67

1 Chapter 1: Introduction

Chapter 1 provides an understanding of basic knowledge of plasma physics that lies behind different parts of this thesis. This chapter starts with the basic plasma physics followed by underlying modelling methods for plasma beams. The motivation and problem definition are then explained. Further, the objectives are defined together with some detailed sub-objectives. Finally, the innovation and contribution are presented before the thesis outline.

1.1 Basic Plasma Physics

In the past, researchers stated that most of matter in the universe was plasmas. Today, researchers again state that most of visible matter in the universe is plasmas. Plasma physics covers a wide scale ranging from the atomic to the meta-galactic^[1], so that it helps us understand connections between microscopic and macroscopic phenomena.

1.1.1 Definition of Plasma

We cannot say that any ionized gas is a plasma since any gases have a small degree of ionization. An effective definition is recognized as follows^[2]:

A plasma is a quasi-neutral gas of charged and neutral particles which exhibits collective behavior.

There are three fundamental parameters that characterize plasmas: (a) the particle density, n ; (b) the temperature, T ; and (c) the magnetic field, B . A large number of subsidiary parameters related to the three parameters, such as Debye length, Larmor radius and thermal velocity, can be derived from these three fundamental parameters. The range of plasmas^[1] is shown in **Figure 1-1(a)**, which shows that solids, liquids and gases exist over a range of electron density and temperatures. For example, in **Figure 1-1(b)**, lightning is an example of plasmas on the earth.

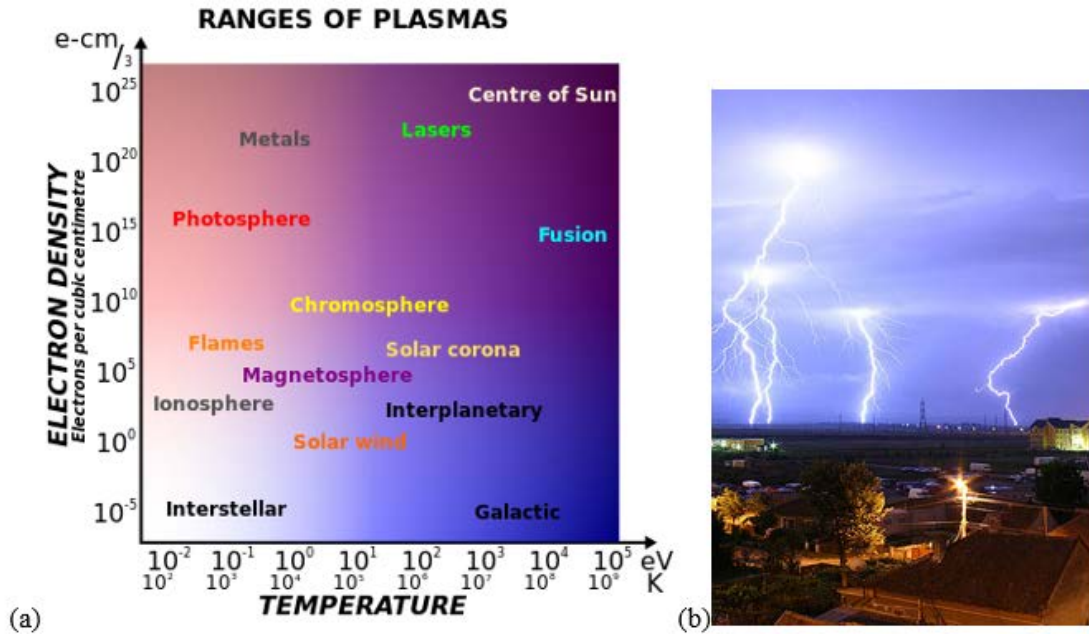


Figure 1-1: Range of Temperature and Density of Plasmas; (b) Lighting over Las Cruces, New Mexico.

1.1.2 Application of Plasma Physics

A plasma is characterized by the two parameters: n and κT in industrial applications, where κ is the Boltzmann constant ($1.3807 \times 10^{-23} \text{J/K}$). There are three typical applications of plasma physics^[3]:

1. **Gas Discharges:** gas discharges are applied in microelectronics industry, materials technology, light industry, analytical chemistry and medical applications;
2. **Thermonuclear Fusion:** thermonuclear fusion is mainly achieved by a deuterium-tritium fusion reaction. When the Lawson criterion is satisfied and temperature is extremely high, particles in a plasma are able to overcome the Coulomb barrier to fuse together.
3. **MHD Generator:** a MHD generator produces electricity by using a plasma jet, in which charged particles are propelled across magnetic fields to the electrodes. Therefore, an electrical current is produced, as shown in **Figure 1-2**.

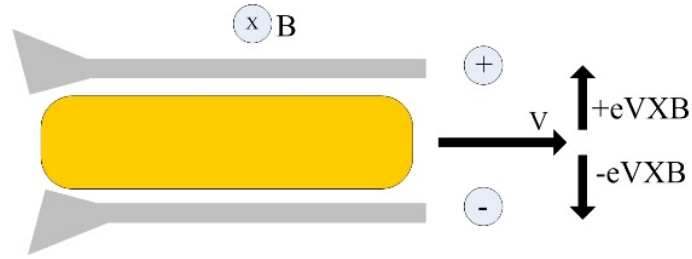


Figure 1-2: Principle of MHD Generator

1.2 Plasma Modelling Methods

There are three main computational simulation methods to investigate high-current plasma beams: fluid, kinetic and hybrid models. In the fluid model, there are charged particles, whose continuity and momentum equations are simultaneously solved with Poisson's equation for electric fields. Additionally, the fluid model is self-consistent and fast compared with the kinetic model. Nevertheless, it occasionally leads to lose local thermodynamic equilibrium (LTE). Alternatively, it is appropriate to apply the kinetic model, which includes Particle-In-Cell (PIC) and Vlasov simulations. For example: PIC simulations retain kinetic features of plasmas, however, they suffer from limited dynamical range and statistical noise, and generally ignore collisions; Vlasov simulations provide a low noise modeling of dynamics. Finally, the hybrid model is a combination of fluid and particle model, in which slow electrons and ions are modeled as fluids; and fast electrons are simulated by employing the MC method for collisions. Therefore, this hybrid model has the advantage of using both the particle and fluid models.

1.3 Motivation

There are two main factors which motivate people to find new computational modelling based on existing MHD and MC methods: (a) because of the complexity of plasma physics, the traditional plasma computational methods have some limitations. For example, the traditional PIC method, which is a collisionless plasma simulation, has modeled plasma particle collisions in a limited way; (b) both intuition and experience

are insufficient to predict plasma dynamics to desired level of accuracy and experimental characterization of plasma is typically difficult as a result of certain extreme operating conditions. The following advantages motivate us to realize improvements on the traditional methods for plasma computational modelling:

- There is a great potential market to use high-current plasma beams as a source of clean energy in industrial applications.
- New methods will overcome the main limitations in the traditional methods, such as the limited dynamical range, the excessive statistical noise and the non-comparable collision time scale.
- Simulation results from new methods will give people a multi-view way to understand high-current plasma beams.
- There is more need to design and validate experiments of high-current plasma beams in order to further explore unknown plasma dynamics.
- It is important to achieve safe conditions for researchers and operators under extreme plasma operations.

1.4 Problem Definition

Computational modelling is a necessary approach to address many complex and nonlinear problems. Different computational approaches have been used for plasma modelling on different spatiotemporal scale. The MC method is commonly used at the smallest scale in plasma physics, especially particle transport processes and collision. However, the accuracy of the MC method is low because of small sample size and computing margin of error^[4]. Therefore, the MC method is not suitable to be applied to many applications. Although researchers have improved the accuracy of the MC method by using variance reduction techniques, such as partial averaging and importance sampling, the accuracy of the MC method is still a problem. Therefore, things will be done to make some improvements to strengthen the accuracy of the existing MC methods by conducting computational simulations of high-current plasma beams in the MC model.

However, the MC method is only capable of analyzing average properties in a plasma, such as particle trajectories and flux. Besides, the MC method has high statistical noise due to having a small number of particles. Therefore, the MC method is not capable of studying other collective plasma properties, such as pressure and velocity distribution. The MHD method is able to solve magnetohydrodynamic effects on large scale for high-current plasma beams and the noise problems are removed. Nevertheless, there are some assumptions without considering some important factors, such as effects of external magnetic fields. The computational models are not comprehensive. Therefore, things will be done to make some improvements based on the existing MHD methods to consider more effects by executing computational simulations of high-current plasma beams in the MHD model.

Since the high-current plasma beams exhibit strongly coupled interaction among electron and ion transports and collisions, electromagnetic fields and fluid flow, there is no reason to completely separate the MHD and MC methods (full discussion is in **Section 2.4**). Fortunately, researchers made efforts to provide hybrid methods by combining the MHD and MC methods. For example, some people used the MHD method to first access initial distribution data, the MC method used those data to predict resultants later. However, the hybrid methods still have gaps in the field of connecting the MHD and MC methods. Therefore, an IMHDMC method is proposed to closely merge the MHD and MC methods together by running computational simulations of high-current plasma beams in the IMHDMC model.

1.5 Objectives

The main goal of the thesis is to simulate high-current plasma beams by employing the new MHD, MC and IMHDMC methods. Besides, the thesis will provide strong plasma simulation foundations for industrial applications. To achieve these goals, the following main objectives are identified:

- i. Develop a new MHD method and implement simulations of high-current plasma beams.
- ii. Develop a new MC method and execute simulations of high-current plasma beams.
- iii. Develop an IMHDMC method and run simulations of high-current plasma beams.
- iv. Verify the three methods by the experimental data and discuss simulations from the MHD, MC and IMHDMC methods.
- v. Discuss the two industrial applications of high-current plasma beams: plasma gasification and fusion energy generation.

The following are detailed sub-objectives of the five main objectives:

➤ **In order to achieve the objective i, we need to do the following tasks:**

1. Develop appropriate assumptions for the new three-dimensional (3D) MHD model in order to consider more important factors in the MHD model.
2. List governing equations for the MHD model, including conservation equations, Ohm's law, Faraday's law and Ampere's law.
3. Design computational domain and boundary conditions based on the MHD model;
4. Adopt appropriate transport coefficients and thermodynamic properties from previous research experiments.
5. Generate fine grids by Gambit software and then simulate the MHD model by ANSYS FLUENT MHD module to acquire effective results.
6. Analyze high-current plasma beams behavior based on the MHD simulations and conclude from the analysis.

In order to achieve the objective ii, we need to do the following tasks:

1. Develop a new MC flowchart including detailed steps to be followed in the whole thesis.
2. Develop an innovative MC algorithm based on simulations of electron transport processes and collisions.

3. Design a 3D MC model using electric and magnetic fields, transport processes and collisions. The electron motion equations, energy and direction should be correctly determined.
4. Develop similar geometries for high-current plasma beams by the PHITS;
5. Apply initial parameters to MC codes and obtain particle properties, such as electron flux, heat and deposit energy.
6. Calculate relative errors to verify the MC simulations produced by the PHITS.

In order to achieve the objective iii, we need to do the following tasks:

1. Develop an IMHDMC flowchart to combine the MHD and MC models.
2. Discover all types of species and related cross sections, as well as basic plasma processes in the IMHDMC model.
3. Develop MHD and MC algorithms in the IMHDMC model.

In order to achieve the objective iv, we need to do the following tasks:

1. Present the experimental data of the HOPE Innovations Inc. (HOPE)'s experiment.
2. Compare the three method simulation results with the experimental data in term of quantitative and qualitative aspects to find if the three methods are consistent with the experiment.
3. Firstly compare the MHD and MC methods and then discuss the three methods in terms of theoretical and simulation aspects.

In order to achieve the objective v, we need to do following steps:

1. Discuss how a Z-pinch works based on a basic explanation.
2. Introduce a new concept of fusion energy generation by intersecting high-current plasma beams and display the HOPE fusion model.
3. Display main parts of a plasma gasification application and a detailed waste processing using the plasma gasification.

1.6 Innovation / Contribution

We have known that the main goal is to develop the new MHD, MC and IMHDMC computational methods for high-current plasma beams, which would be used to understand complex plasma phenomena in industrial applications. The thesis contributes to model and simulate high-current plasma beams by the three new methods.

The innovation and contributions in this thesis are as follows:

- ✚ This thesis puts specific emphases on plasma computational simulations by the three new methods: MHD, MC and IMHDMC.
- ✚ In the MHD model, the external magnetic fields are considered; and the conversation equations, Ohm's law, Faraday's law and Ampere's law are solved. Besides, the transport coefficients and thermodynamic properties are obtained from verified experimental data that help us approach reliable models.
- ✚ In the MC model, we use an advanced MC algorithm and the Null-Collision technique. By enabling process of tracing electrons using appropriate data, the MC method investigates both electron transport processes and collisions in a random manner.
- ✚ A new hybrid method, the IMHDMC method, is reasonably proposed to combine the MHD and MC models. It not only eliminates gaps between the MHD and MC models but also closely links them.
- ✚ The three method simulation results are verified by the HOPE's experimental data in terms of quantitative and qualitative aspects. The verification proves that the three new computational methods are correct.
- ✚ The comparison and discussion based on the MHD, MC and IMHDMC methods are highlighted. We can choose appropriate methods to solve plasma problems.

1.7 Thesis Outline

The thesis is organized into six chapters. The introduction, including the basic plasma physics and modelling methods for a plasma, motivation, problem definition, objectives, and innovation/contribution, are depicted in **Chapter 1**. In **Chapter 2**, the literature review is an important part and it shows us some previous reference papers from researchers. In **Chapter 3**, the MHD, MC and IMHDMC methods are investigated for the high-current plasma beams. In **Chapter 4**, the MHD, MC and IMHDMC simulation results are presented and the experimental verification for the three methods are shown quantitatively and qualitatively. In **Chapter 5**, the comparisons between the MHD and MC methods are given. The discussions between the three methods are obtained from the theoretical and simulation aspects. Finally, the conclusion of overall work, the potential applications and the future work are discussed in **Chapter 6**.

2 Chapter 2: Literature Review

In **Chapter 2**, overall theoretical descriptions of plasma simulations are first depicted, as shown in **Figure 2-1**. The three computational modelling approaches of a plasma are presented: (a) using the computational fluid dynamics (CFD) commercial codes based on the MHD theory; (b) using the PHITS^[5] codes based on the MC theory; and (c) using the IMHDMC method based on the MHD and MC models. Finally, plasma diagnostic technologies are briefly introduced.

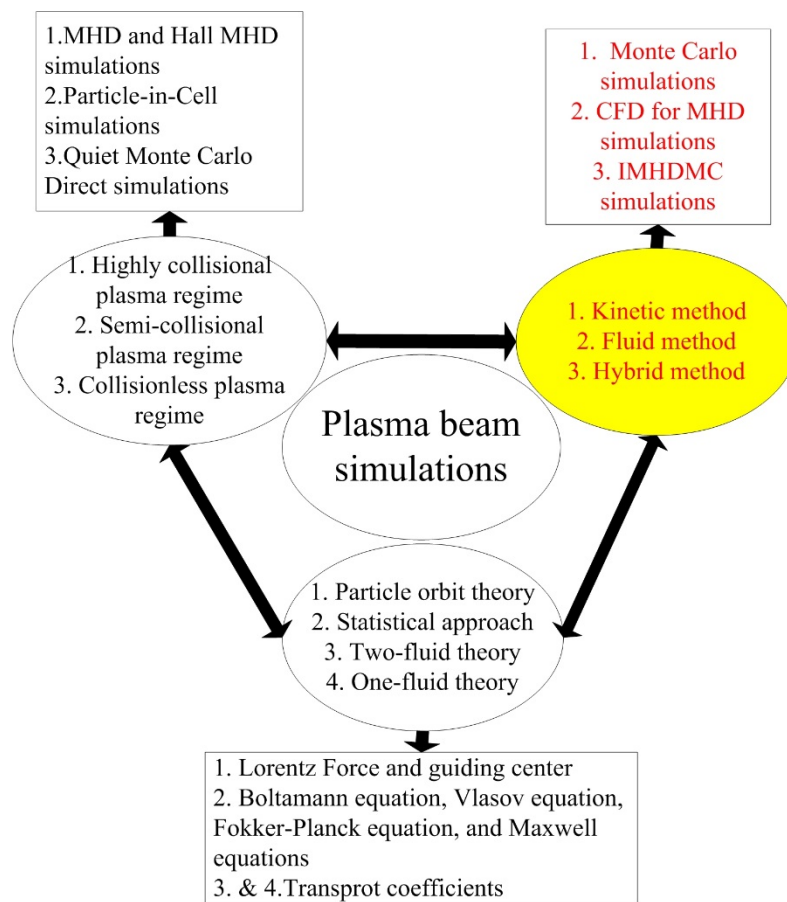


Figure 2-1: Overall Theoretical Descriptions of Plasma Simulations

2.1 Theoretical Descriptions of Plasma Phenomena

Dynamics of a plasma are mainly governed by interactions between charged particles, internal fields and external fields. As the charged particles, such as electrons and ions, move around in the plasma. They generate local concentrations of negative or positive

charges that produce electric fields. Further, charged particle motion generates electric currents and magnetic fields. The characteristics of the plasma are analyzed by the classical mechanics law, which is non-quantum. Since quantum effects are only studied at very high densities and very low temperatures^[6].

2.1.1 Self-Consistent Formulation

Interactions between charged particles and electromagnetic fields are governed by the Lorentz force. For a charged particle with a mass, m , which moves with velocity, \vec{v} , in an electric field, \vec{E} , and a magnetic field, \vec{B} , the equation of the Lorentz force, \vec{F} , is

$$\vec{F} = q(\vec{E} + \vec{v} \times \vec{B}) \quad (2.1)$$

where q is the elementary charge ($1.602 \times 10^{-19}\text{C}$).

It is important to depict dynamics of a plasma by solving the equations of motion and Maxwell's equations for each particle in the plasma. Therefore, we start a discussion of plasma dynamic equations with electrodynamics. If we have a total number of particles N , we will have N nonlinear coupled differential motion equations to simultaneously solve. A self-consistent formulation is provided since electromagnetic fields and charged particles are intrinsically coupled. Maxwell's equations are as follows:

$$\nabla \times \vec{E} = -\frac{\partial \vec{B}}{\partial t} \quad (2.2a)$$

$$\nabla \times \vec{B} = \mu_0 \left(\vec{J} + \epsilon_0 \frac{\partial \vec{E}}{\partial t} \right) \quad (2.2b)$$

$$\nabla \cdot \vec{E} = \frac{\rho}{\epsilon_0} \quad (2.2c)$$

$$\nabla \cdot \vec{B} = 0 \quad (2.2d)$$

Where $t, \rho, J, \epsilon_0, \mu_0$ denote the time, the charge density, the current density, the electric permittivity and the magnetic permeability.

Equation 2.2a is Faraday's law that states that a time-varying magnetic field induces a

rotation of an electric field. **Equation 2.2b** without $\frac{\partial \bar{E}}{\partial t}$ term is Ampere's law and this term $\frac{\partial \bar{E}}{\partial t}$ is the displacement current. **Equation 2.2c** is Gauss's law for electric fields, which tells us that electric lines begin or end on charges. **Equation 2.2d** is Gauss's law for magnetic fields, which represents that there are no magnetic monopoles. Maxwell's equations provide us an effective tool to study electromagnetic phenomena.

2.1.2 Theoretical Approaches for Plasma Simulation

There are the three principal theoretical approaches with corresponding approximations in different circumstances for plasma simulations: one-fluid theory, statistical approach and two-fluid theory. The three theoretical approaches^[7] are illustrated below:

1. *One-fluid Theory*

This approach treats a plasma as a single conducting fluid, which uses macroscopic variables and corresponding hydrodynamic conservation equations. A simplified form is a MHD approximation model, which is useful to study very low frequency phenomena in conducting fluids immersed in magnetic fields.

2. *Statistical Approach*

Since a plasma contains large interacting charged particles, it is appropriate to adopt this approach in order to provide a macroscopic description for the plasma. The problem is based on solving the kinetic equations that determine evolution of distribution function in phase space. The typical kinetic equation is Vlasov equation, in which interactions between charged particles are depicted by electromagnetic fields consistent with distribution of current (charge) density inside a plasma.

3. *Two-fluid Theory*

When collisions between particles in a plasma are very frequent, it means that each species is capable of maintaining the LTE in the two-fluid theory. The each species is then regarded as a fluid, which has a local density, macroscopic velocity and temperature. Alternatively, a plasma becomes a mixture of two interpenetrating fluids. In addition to electrodynamic equations, a set of hydrodynamic equations are used to

express conservations of mass, energy and momentum for each species in a plasma.

On the one hand, theoretical descriptions of plasma phenomena can be as simple as a valid model. On the other hand, they can be also as complicated as some coupled partial differential equations. The plasma theoretical methods, tools and references are shown in **Table 2-1**.

Table 2-1: Three Main Approaches for Plasma Simulations

Method	Tool	References
One-fluid theory	CFD MHD module	Katerina Horakova and Karel Frana (2011); A Lebouvier et al. (2013); Beycan Ibrahimoglu et al. (2014)
Statistical approach	MCNP ^a , PHITS, and PENELOPE ^b	Jun Li et al.(1995); C. Theis et al. (2006); C Kirkby et al. (2008); E. G.Sheikin (2010); Koji Niita et al. (2010)
Hybrid method	CFD and MCNP	Fawaz Ali (2009); Qing Yang (2013); Hossam A. Gabber et al. (2015)

^aMCNP denotes Monte Carlo N-Particle.

^bPENELOPE denotes Penetration and ENergy Loss of Positrons and Electrons.

2.2 MHD Modelling for Plasmas

The MHD method is concerned with mutual interactions between fluid flow and magnetic fields. The mutual interactions of magnetic and velocity fields happen due to Ohm's law, Faraday's law, Ampere's law and the Lorentz force.

2.2.1 MHD Conservation Equations

The behavior of a plasma in industrial applications is depicted by a simplified model, in which a plasma is regarded as a quasi-neutral fluid and electrical charges with the Maxwell distribution function. Besides, interactions and fluid element motion are also considered. The MHD equations mainly derived from the conservation equations, as shown in **Table 2-2**.

Table 2-2: MHD Equations

Faraday's law	$\frac{\partial \vec{B}}{\partial t} = -\nabla \times \vec{E}$
Ampere's law	$\nabla \times \vec{B} = \mu_0 \vec{J}$
Conservation of mass	$\frac{\partial \rho}{\partial t} + \vec{v} \cdot \nabla \rho = 0$
Conservation of momentum	$\frac{d \rho \vec{v}}{dt} = -\nabla p + \vec{J} \times \vec{B}$
Adiabatic equation for a fluid	$\frac{d}{dt} \left(\frac{p}{\rho^{\gamma_h}} \right) = 0$
Ohm's law	$\vec{E} + \vec{v} \times \vec{B} = 0$ or $\vec{E} + \vec{v} \times \vec{B} = \eta \vec{J}$

where p is the pressure, γ_h is the heat capacity ratio and η is the electrical resistivity.

Assume that collisions are sufficient to ensure that the pressure is isotropic. In practice, the following conditions must be satisfied:

- Mean-free-path \ll Interested length scale
- Larmor radius \ll Interested length scale
- Collision time \ll Interested time scale

Some source terms, such as radiation and gravity, are all missed.

2.2.2 Examples for 3D MHD Modelling

Numerical studies, which simulate coupled phenomena between a conductive fluid and electromagnetic fields, are performed by a finite volume method (FVM) and a finite element method (FEM) in some commercial codes, such as COMSOL, ANSYS CFX and FLUENT modules^[8]. The use of these CFD codes is beneficial to understand the plasma phenomena in a complex geometry. In the 3D MHD modelling, plasmas have been numerically evaluated using the effective computational tools as follows:

1. *3D MHD Modelling of A Direct Current (DC) Low-Current Plasma Arc Batch Reactor at Very High Pressure in Helium*^[9]

This paper builds a 3D time-dependent MHD model under unusual conditions: very high pressures (from 2MPa up to 10MPa) and low currents ($<1A$). The mathematical model includes four main steps: (a) the first step gives main assumptions according to

the 3D time-dependent MHD model; (b) the second step gives us the governing equations, which are Navier-Stokes equations; (c) the third step shows boundary conditions and other related parameters; and (d) the fourth step gives us appropriate transport coefficients and thermodynamic properties for a helium gas. The model is built based on the previous model for a non-transferred flow plasma torch, which is used for hydrocarbon reforming. After that, the previous model is modified to work at very high pressures and low currents in a batch reactor.

2. Numerical Modelling of DC Arc Plasma Torch with MHD Module^[10]

In this paper, ANSYS FLUENT MHD module^[11] is used to simulate a fluid flow in electromagnetic fields. The model is based on assumptions for numerical modelling of heat, mass, electromagnetic fields and a fluid flow in a plasma torch. The fluid is considered as a continuum plasma gas in the LTE condition. The author uses three conservation equations and provides the MHD theory. The electric potential method is used due to its easiness of solving source terms with one equation. The plasma modelling geometry is a SG-100 torch with five parts. The calculations are performed after the torch model is meshed using 175000 tetrahedral cells that have 0.203 skewness value. The realizable K-epsilon ($k-\varepsilon$) turbulence model^[12] is chosen for turbulent fluid in this model. The $k-\varepsilon$ turbulence model is a two equation model which gives us a general turbulence description by means of two partial differential transport equations (PDEs): (a) turbulent kinetic energy equation and (b) dissipation equation. All boundary conditions are given. In the results and discussion, the author concludes that the Joule heat and Lorentz force are the main parameters which affect the fluid flow in magnetic fields.

3. Three-Dimensional Modeling of Plasma ARC in ARC Welding^[13]

The author builds a mathematical model and shows us how to simulate it after solving 12 differential equations for an arc welding process. In order to solve all equations in addition to the conservation equations, a 3D plasma arc model is simulated. The Semi-Implicit Method for Pressure-Linked (SIMPLE) algorithm is applied to solve the conservation equations of momentum and mass. In order to make a steady state solution,

the set of differential equations are solved by the following algorithm: (1) the continuity conversation equation is first solved based on updated properties; (2) current density and source terms for Poisson's equation are then calculated; (3) using the magnetic fields solved, the Lorentz force is calculated for the momentum conservation equation; (4) the conservations of mass and momentum are solved to obtain pressure and velocity fields; (5) the conservation of energy is solved to obtain new temperature distribution; and (6) T-dependent properties are updated and the program iterates to the first step. The above-mentioned algorithm continues until a converged solution is reached.

2.3 MC Modelling for Plasmas

2.3.1 Examples for MC Modelling

1. Monte Carlo Simulation of Nonequilibrium Conductivity Produced by Electron Beam in MHD Flow^[14]

Fast MC codes are developed for a calculation of deposit energy in a form of spatial distribution by an electron beam (e-beam) in a substance. The conductivity in a MHD flow is sustained by e-beam. In order to obtain electron concentrations, deposit power density in the MHD flow is used as a main characteristic of the e-beam. The self-consistent formulation uses iteration procedures and is realized for simulations of the MHD flow with non-equilibrium conductivity sustained. Conductivity is one of main characteristics of plasma, which is determined by electron concentration, n_e , and electron mobility, μ_e , by the relation $\sigma = e\mu_en_e$, where e is the electron charge. An approach in which the electron concentrations in a plasma are changing, just considers along the direction of flow velocity. Finally, the MHD flow over a plate and wedge has been calculated and analyzed under different conditions.

2. Estimation of Amount of Scattered Neutrons at Devices PFZ and GIT-12 by MCNP Simulations^[15]

This paper is dedicated to the pinch effect occurring during a current discharge in a deuterium plasma. During fusion reactions that proceed in the plasma during the

discharge, neutrons are produced. The authors use neutrons as an instrument for plasma diagnostics. Despite of an advantage that neutrons do not interact with electric and magnetic fields inside the device, we use the MCNP code to estimate rate of neutron scattering. The main problem of defining parameters for the simulations in MCNP is to sufficiently define the geometry of experimental setup to realize as a realistic model as possible. User of this program creates the input file where the considered geometry, materials, particle sources, type of results and number of iterations are defined. There are the MCNP results for PFZ and GIT-12 devices, which are commercial products. In the first device, the authors calculate neutron energy spectrums in the three places where they put probes in the experimental setup. In the second device, the authors simulate neutron energy spectrums in the places of two scintillation probes: (a) one is axially placed 10.12m above the neutron source (D_1) and (b) the other is radially in the same distance (D_2). Finally, relative inaccuracy of the results is 0.2 %.

2.4 Hybrid Modelling for Plasmas

When we combine various methods, such as the MHD and MC methods, to simulate a plasma, it is known as a hybrid method. Indeed, there are three main types of hybrid methods: (a) one kind of hybrid method models low-energy electrons using a fluid model, while high-energy electrons, which can lead to excitation and ionization processes, are simulated using MC techniques; (b) other hybrid method uses the PIC method for kinetic treatment of species and particles are studied on a continuous mesh. However, other species are simulated with a fluid model. Average particle properties and electromagnetic fields are calculated on a fixed discrete mesh; and (c) another hybrid method treats different parts of a plasma geometry in different ways. For example: researchers usually combine MC techniques for non-thermal electrons with fluid models in some parts and for species motion in other parts.

2.4.1 Examples for Hybrid Methods

1. *On The Integration of CFD Simulations with MC Radiation Transport Analysis*^[16]

Numerous scenarios exist whereby radioactive particulates are transported between spatially separated points of interest. A typical example related to phenomena is the resuspension of radioactive particulates from resultant fallout fields, in the aftermath of a Radiological Dispersal Device (RDD) detonation. Quantifying spatial distribution of radioactive particulates allows for calculations of potential radiation doses, which can be incurred from exposure to such particulates. Presently, there are no simulation techniques that link the radioactive particulate transport with the subsequent radiation field determination. The paper develops a coupled CFD and MC Radiation Transport approach to solve the problem. Via particulate injections, CFD simulations define the spatial distribution of radioactive particulates. After that, this distribution is employed by MC simulations to characterize resultant radiation fields. GAMBIT and ANSYS FLUENT are employed for the CFD simulations, while MCNPX is used for MC Radiation Transport simulations.

2. *A Computational Fluid Dynamic Approach and MC Simulation of Phantom Mixing Techniques for Quality Control Testing of Gamma Cameras*^[17]

In order to reduce unnecessary radiation exposure for clinical personnel, the optimization of procedure in a quality control test of gamma camera is investigated. Firstly, a CFD model is investigated to simulate the mixing procedure. Mixing techniques of shaking and spinning are simulated using the CFD tool ANSYS FLUENT. In the second part of this study, a Siemens ECAM gamma camera is simulated using the MC software SIMIND. A series of validation experiments demonstrate the reliability of MC simulations. In the third part of this study, the simulated mixing data from ANSYS FLUENT is used as source distribution in the SIMIND to simulate a tomographic acquisition of a phantom. The planar data from the simulations is reconstructed using filtered back projections to produce a tomographic data set for activity distribution in the phantom. This completes the simulation routine for the

phantom mixing and verifies the Proof-in-Concept that the phantom mixing problem can be studied using a combination of CFD and nuclear medicine radiation transport simulations.

2.5 Plasma Diagnostic Technology

Plasma properties to be measured include density, temperature, thermal conductivity, distribution function and stability or instability of a plasma. Generally, some of these properties are related and a measurement of one determines one or more of the others. For example, Langmuir and Mott-Smith developed the theory of electrostatic probes as shown in **Figure 2-2**. A Langmuir electrostatic probe is mainly used to measure electron and ion density, electron temperature and plasma potential. Besides, magnetic probes are used to sample magnetic fields in or around plasmas. These magnetic probes operate on the principle that time-changing magnetic fields induces a voltage in loops and the magnetic fields can be determined from a measurement of an induced voltage.



Figure 2-2: Langmuir Electrostatic Probe^[18]

3 Chapter 3: Methodology

In **Chapter 3**, we derive the comprehensive models for high-current plasma beams using the MHD, MC and IMHDMC methods. We briefly describe the methodology for the MHD, MC and IMHDMC methods in **Section 3.1**. Motivated by these, we start to describe plasma dynamics by developing the MHD, MC and IMHDMC models in **Section 3.2**, **Section 3.3** and **Section 3.4**.

3.1 Methodology for High-Current Plasma Beams

High-current plasma beams are produced by a DC discharge, which is sustained through secondary electron emission at the cathode due to ion bombardments. After electrons are ejected from the cathode, they are also accelerated into an argon gas. The electrons acquire enough energy to ionize the argon gases and create new electron-ion pairs at the same time. When the electrons attain the anode, the ions migrate to the cathode where they create new secondary electrons.

Most importantly, the Knudsen number (Kn) is an important reference in the thesis. The Kn is defined as the ratio of the molecular mean free path length to the representative physical length scale as follows^[19]:

$$Kn = \frac{\lambda_m}{L_r} \quad (3.1)$$

where λ_m denotes the mean free path and L_r denotes the representative physical length scale.

The Kn is useful to determine whether the statistical mechanics or the continuum mechanics should be used: (a) if the Kn is close to or greater than 1, statistical methods, such as the MC method, must be used. Since a continuum method does not explain microscopic interactions in a plasma despite its accuracy; and (b) if the Kn is less than

1, continuum methods, such as the MHD method, must be used.

3.1.1 Flowchart for MHD Method

The coupled flow fields and electromagnetic fields are explained on the two main effects: (a) the induction of electric current due to movement of conducting fluid in magnetic fields and (b) the Lorentz force as the result of the electric current and magnetic field interactions. Generally, the induced electric current and the Lorentz force tend to oppose the mechanisms that create them. Stirrings of fluid movements are produced by the Lorentz force. In **Figure 3-1**, the two effects are considered in the MHD flowchart.

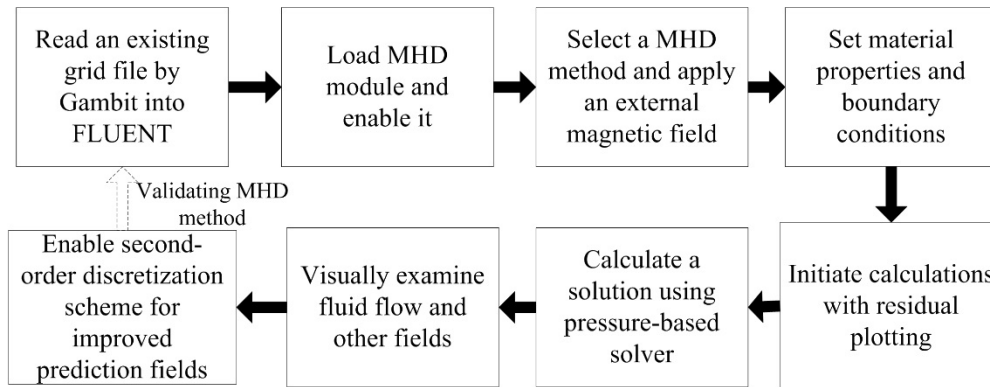


Figure 3-1: MHD Flowchart by ANSYS FLUENT and Gambit for High-current Plasma beam

3.1.2 Flowchart for MC Method

In the MC method, the high-current plasma beams are simplified as beams that are ionized to plasma state by an e-beam source in electric and magnetic fields. The PHITS is not only used to build and visualize geometries of the plasma beams, but also used to develop the e-beam source and calculate the electron flux, heat and deposit energy parameters. Besides, the PHITS provides relative error function to help us check calculations. The detailed MC flowchart is depicted in **Figure 3-2**.

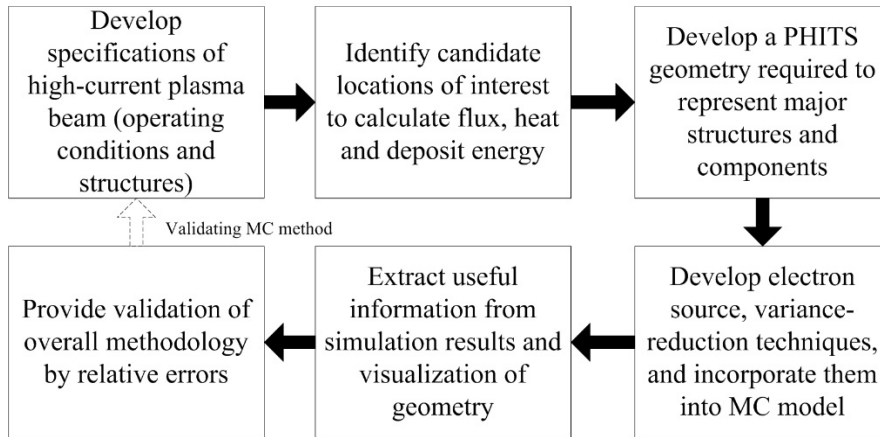


Figure 3-2: MC Flowchart by PHITS for High-Current Plasma Beam

3.1.3 Flowchart for IMHDMC Method

Figure 3-3 illustrates the three parts in the IMHDMC method: the general input; the coupled and interacting MHD and MC models; and the final output. Once we obtain MHD and MC simulations, the IMHDMC method is used to integrate the simulation results in order to obtain realizable plasma properties. Finally, the simulation results from MHD and MC models are also validated by the IMHDMC method.

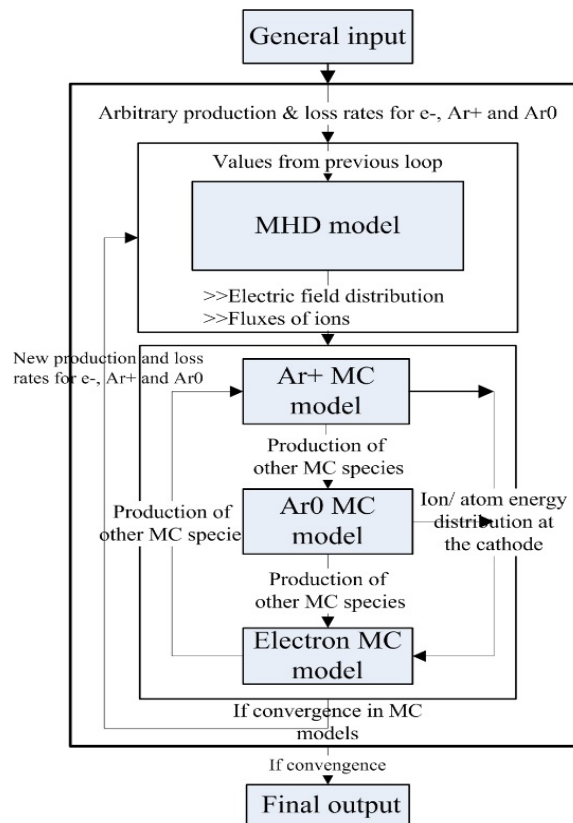


Figure 3-3: IMHDMC Flowchart for High-Current Plasma Beam^[20]

3.2 MHD Numerical Modelling

In order to study the dynamics of the high-current plasma beams, the MHD model built by the ANSYS FLUENT MHD module is shown in **Figure 3-4**.

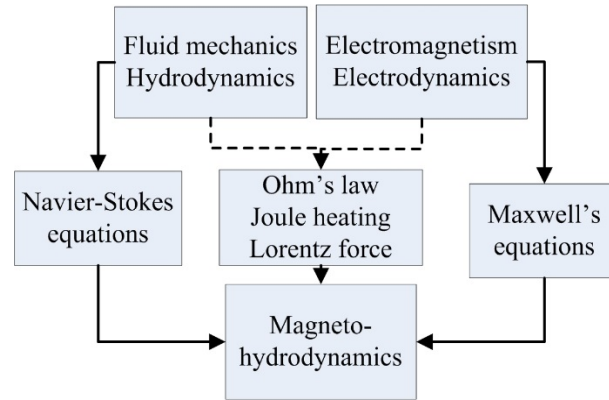


Figure 3-4: MHD Model for High-Current Plasma Beam

3.2.1 Assumptions

The 3D MHD model has the following assumptions^{[21][22]}:

- The magnetohydrodynamic fluid is treated as a steady, turbulent, compressible viscous and single continuous flow in the LTE.
- The plasma beams are assumed to be fully ionized and quasi-neutral, which mean that the number of electrons is equal to the number of ions in plasma beams.
- The induced current as a transient term is small compared to the injected current so it is consequently neglected. The induced magnetic field is also neglected due to a small magnetic Reynolds number^[23] that is equal to 0.15.
- No ferromagnetic materials are presented in the domain and the magnetic permeability for gaseous medium is therefore a constant.
- The argon gas is assumed to be compressible and expandable. Both thermodynamic properties and transport coefficients only depend on temperature.

Two methods, including the electrical potential method and magnetic induction method, can be selected. In this study, the magnetic induction method is used and the solution of governing equations is numerically solved using the ANSYS FLUENT MHD

module.

3.2.2 Governing Equations

Based on the assumptions in **Section 3.2.1**, high-current plasma beams are modeled by a set of following equations: (a) the general mass, energy and momentum conservation equations to describe fluid dynamics and (b) Ohm's law, Faraday's law and Ampere's law to describe electromagnetism. It is necessary to include important source terms in the energy and momentum conservation equations. We therefore add the radiative cooling effects, Ohm's heating, together with the Lorentz force due to self-induced and external magnetic fields. All the equations^{[24][25]} are written in a Cartesian system (x,y,z).

1. Conservation of Mass

$$\frac{\partial \rho}{\partial t} + \vec{v} \cdot \nabla \rho = 0 \quad (3.2)$$

2. Conservation of Energy

$$\frac{\partial \rho h}{\partial t} + \vec{v} \cdot \nabla \rho h = \nabla \cdot \frac{\lambda}{C_p} \nabla h + \vec{J} \cdot \vec{E} - S_{rad} \quad (3.3)$$

3. Conservation of Momentum

$$\frac{\partial \rho \vec{v}}{\partial t} + \vec{v} \cdot \nabla \rho \vec{v} = -\nabla p + \nabla \tau + \vec{J} \times \vec{B} \quad (3.4)$$

4. Ohm's Law

$$\vec{J} = \sigma (\vec{E} + \vec{v} \times \vec{B}) \quad (3.5)$$

5. Faraday's Law and Ampere's Law

$$\frac{\partial \vec{B}}{\partial t} = -\nabla \times \vec{E} \quad (3.6a)$$

$$\nabla \times \vec{B} = \mu_0 \vec{J} \quad (3.6b)$$

where h is the specific total enthalpy, λ is the thermal conductivity, C_p is the specific heat, S_{rad} is the radiation losses, τ is the viscous stress, and σ is the electrical conductivity. The parameters ρ , h, λ , C_p , and σ depend on temperature and are taken from the study^[26] at the atmospheric pressure.

The conservation equations, Ohm's law, Faraday's law and Ampere's law are solved

by the ANSYS FLUENT module. When we apply the Reynolds transport theorem and divergence theorem in the conservation of mass, **Equation 3.2** is obtained. In **Equation 3.3**, the term $\vec{J} \cdot \vec{E} = (1/\sigma)\vec{J}^2$, which is the Ohm's heating term, is produced when an electric current goes through the high-current plasma beams. It is a major factor leading to high temperature of plasma beams. The source term S_{rad} is a radiation and only depends on temperature, which is calculated from the net emission coefficient (NEC)^[27]. The source term $\vec{J} \times \vec{B}$ in **Equation 3.4**, is the Lorentz force, which represents interactions between electric current and magnetic fields.

3.2.3 Boundary Conditions

The geometry for the MHD model is shown in **Figure 3-5** and the MHD model has the three parts: (a) the inlet, (b) the outlet and (c) the conducting wall.

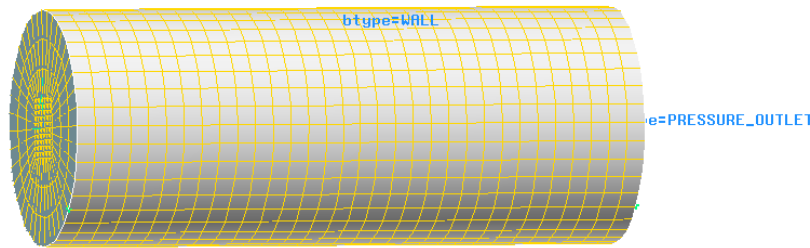


Figure 3-5: Geometry of High-Current Plasma Beam

The cylinder ($r=2\text{cm}$) is parallel to Z-axis and the inlet is parallel to XY cross section. The length of cylinder is 10cm and the total volume of cylinder is $1.25 \times 10^{-4} \text{ m}^3$, which is close to the experimental model. The MHD model includes 7040 cells, 21980 faces and 7953 nodes. The boundary conditions for the MHD model are shown in

Table 3-1. The higher pressure is imposed at the inlet and the temperature of injected argon gas is 1500 K at the inlet. The wall is considered as a conducting wall, which is made of copper. Firstly, an atmospheric pressure and temperature of 300K are applied to the whole conducting wall. The 3D external applied magnetic fields (B_{0x} , B_{0y} , B_{0z}) are also applied in the MHD model.

Table 3-1: Boundary Conditions for MHD Model

	u (m/s)	v (m/s)	w (m/s)	T (K)	p (KPa)	B _{0x} (T.m)	B _{0y} (T.m)	B _{0z} (T.m)
Inlet	0	0	1.2	1500	$\frac{\partial P}{\partial z} = 0$	0.5	0.5	1
Outlet	$\frac{\partial u}{\partial n} = 0$	$\frac{\partial v}{\partial n} = 0$	$\frac{\partial w}{\partial n} = 0$	300	101.3	0.5	0.5	1
Wall	0	0	0	300	$\frac{\partial P}{\partial n} = 0$	0.5	0.5	1

3.2.4 Thermodynamic Properties and Transport Coefficients

The thermodynamic properties and transport coefficients for pure argon are calculated over the temperature range from 300K to 30,000K and under 0.1MPa, which are applied in most thermal plasma processes. The values of viscosity, thermal conductivity and electrical conductivity for pure argon gas are picked from the paper by Murphy and Arundell^{[28][29]}, which are depicted by the solid line in **Figure 3-6**. For pure argon gas, the transport coefficients are calculated according to the equilibrium composition, which conduct the principle of minimization of the Gibbs free energy of the mixture. The thermodynamic properties are obtained by the minimization of the free enthalpy by the RAND method provided by White and Dantzig^[30]. Besides, the NEC of argon plasmas is illustrated in **Figure 3-7**.

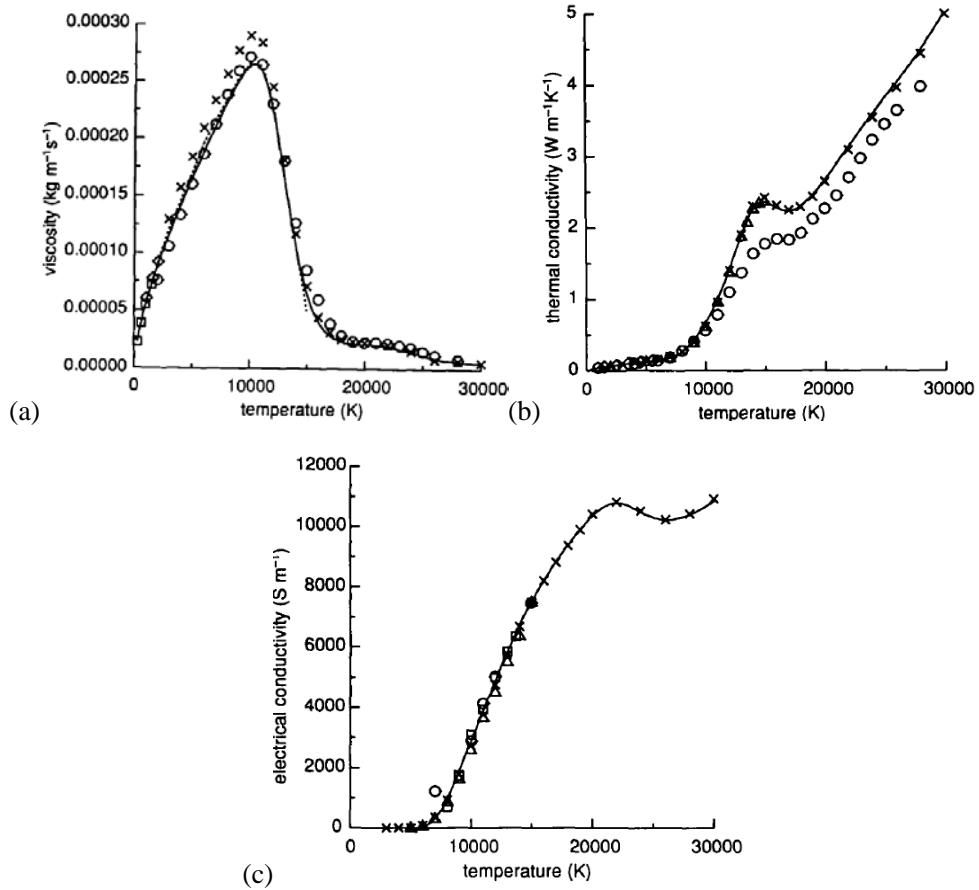


Figure 3-6: (a) Viscosity, (b) Thermal Conductivity and (c) Electrical Conductivity for Argon Gas

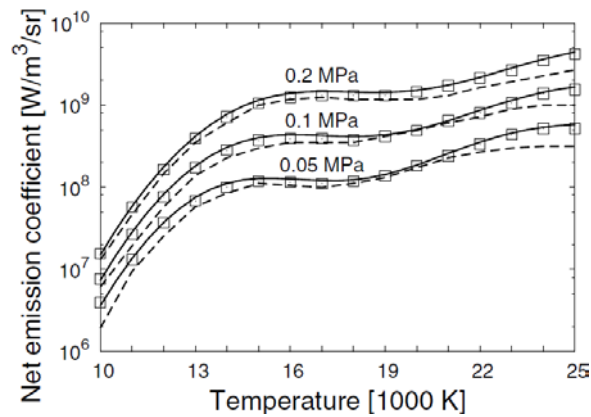


Figure 3-7: NEC of Argon Plasmas Calculated in Reference (—), in Reference^[31] (•) and Measured in Reference^[32]

3.3 MC Numerical Modelling

During chemical reactions in high-current plasma beams, electrons are produced. We present detailed properties of the high-current plasma beams in a DC discharge by the MC simulations. **Section 3.3.1** and **Section 3.3.2** are devoted to the MC numerical modelling.

3.3.1 MC Algorithm

We first consider that an electron crosses more interfaces: starting in one layer and cut off in another layers. Path length is assumed to be obtained by a mean free path in air (68nm)^[33] at an ambient pressure (10^{-3} Pa) and random number in a starting layer. After a while, the path length is then corrected through ratio of mean free paths of the layers that the electron travels.

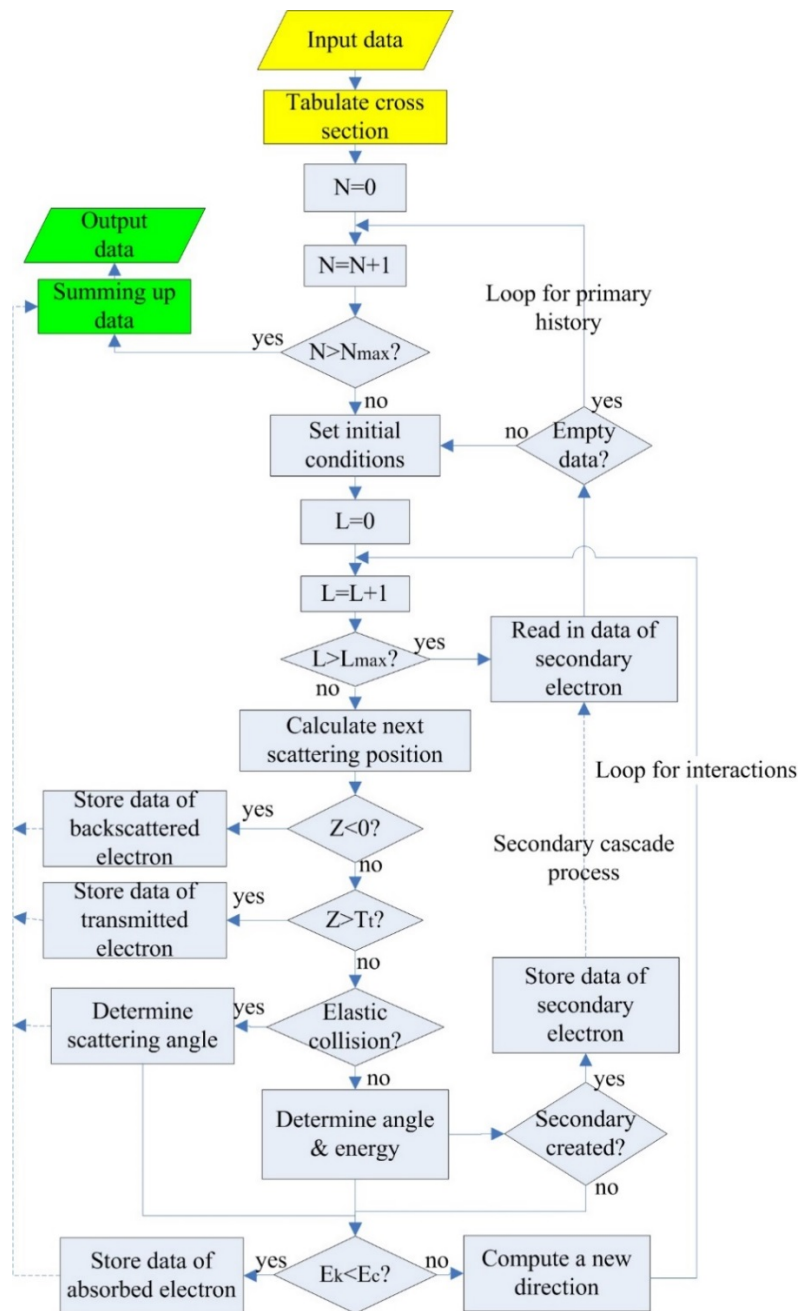


Figure 3-8: MC Algorithm^[34] Permitting Simulation of Primary Electron Trajectories and Secondary Cascade Process in MC Model

where N and L are the number of traced electrons and steps of the tracing electrons (N_{\max} and L_{\max} are the maximum values). E_k denotes the kinetic energy and E_c denotes the cut-off energy. Z denotes the depth of the tracing electrons and T_t denotes the total thickness of sample.

The MC algorithm consists of the three parts, as shown in **Figure 3-8**. The first part shaded by yellow is for the initial conditions, including specifications of a copper wall and an e-beam source and parameters for controlling options. Tables of cross-sections are prepared in advance, such as differential cross-sections as a function of scattering angle and energy loss and total cross-sections. It could be helpful to enable processes of tracing electrons by choosing appropriate data randomly. The second part shaded by blue is the main part of the MC algorithm and includes two steps: (a) the tracing of electrons continuously runs step by step, until cut-off condition is satisfied, and (b) the same steps are executed one by one, up to a total history number, N . The last part shadowed by green is to process the accumulated results derived from the second part simulations and outputs these updated data into fields.

3.3.2 Detailed MC Model

The PHITS simulates each particles using the MC method. In **Figure 3-9**, the tallies are used to estimate average behavior of particles, such as particle flux, heat and deposit energy^[35]. Besides, other physics quantities can be deduced from PHITS simulations.

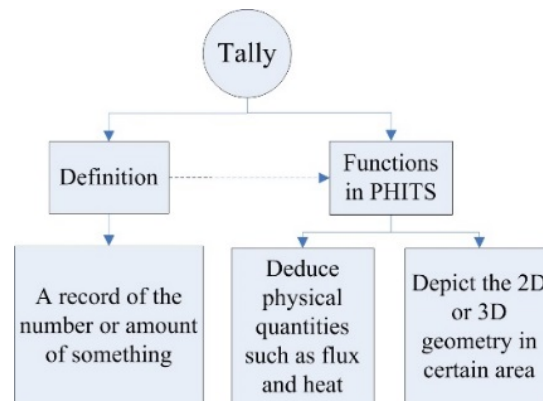


Figure 3-9: Tally's Definition and Functions in PHITS

In **Section 3.3.2**, the 3D MC model is used to investigate electron motion in high-

current plasma beams. Electrons propagating in the high-current plasma beams perform elastic and inelastic collisions with argon atoms, which change electron energy and moving direction. The MC method is based on the Null-Collision technique^{[36][37]}, which is not same as that of Razdan et al.^{[38][39]}, where a path-length technique is used.

3.3.2.1 Electric and Magnetic Fields

The MC model^[40] for the high-current plasma beams is shown in **Figure 3-10**, where electric fields are assumed to be uniform and magnetic fields are assumed to be time-independent in space. Besides, the X and Y magnetic fields, B_x and B_y , are transverse to the electric fields, but the Z magnetic field, B_z , is opposite to the electric fields. An argon gas is assumed to have uniform density throughout the cathode region at the temperature of 300 K.

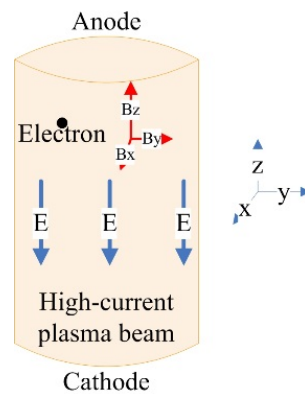


Figure 3-10: MC Model for High-Current Plasma Beam

3.3.2.2 Transport Processes and Collisions

Initial electrons emitted from the cathode starts in the MC simulations. For an initial electron with an initial position ($x = 0, y = 0, z = 0$), it is assumed to have an initial projectile energy (158 keV). Entry angle is randomly selected in line with a cosine distribution. The electrons are assumed to freely move until an arbitrary collision happens and flight time between two successive collisions is calculated by the Null-Collision technique. There are the three components in the magnetic fields including the B_x , B_y , and B_z . The electron motion equations between two collisions are shown in

Table 3-2.**Table 3-2:** Electron Motion Equations^[41] in MC Model

Electron motion equation	B _x	B _y	B _z
v _x	0	$\frac{dv_x}{dt} = -\omega_c v_z$	$\frac{dv_x}{dt} = \omega_c v_y$
v _y	$\frac{dv_y}{dt} = \omega_c v_z$	0	$\frac{dv_y}{dt} = -\omega_c v_x$
v _z	$\frac{dv_z}{dt} = \frac{e}{m_e} (E - v_y B)$	$\frac{dv_z}{dt} = \frac{e}{m_e} (E + v_x B)$	$\frac{dv_z}{dt} = \frac{e}{m_e} E$

where v_x, v_y and v_z, denote the velocity along the x, y and z direction, m is the electron mass, $\omega_c = eB / m$ is the cyclotron frequency and $v_c = \omega_c / 2\pi$.

The electron motion equations are integrated using a fourth order Runge-Kutta routine. At the end of time step, a random number uniformly distributed between 0 and 1 is used. When the random number is less than probability of a collision, the collision is real, otherwise the collision is null. In such cases, we go to next collision without any change in electron energy. For real collisions, the same random number is used to determine whether it is an elastic, excitation or ionization collision. The electron energy is changed as follows^[42]:

$$\xi = \begin{cases} \xi_0 \\ \xi_0 - \xi_{exc} \\ (\xi_0 - \xi_{ion}) / 2 \end{cases} \quad (3.7)$$

where ξ_0 is the initial energy of electrons before collisions and also the energy for elastic collisions; ξ_{exc} and ξ_{ion} are the excitation and ionization threshold energies.

We assume that electrons generated during ionization have zero energy and ion motion is neglected. The energy of electrons after a collision can be used as starting condition for free motion of the electrons until next collision (energy of an electron after an elastic collision is equal to its energy before the collision). Based on larger cross sections of

elastic collisions, the electrons are assumed to be isotropically scattered and new direction is determined by:

$$\cos \theta = 1 - 2N_1 \quad (3.8)$$

$$\varphi = 2\pi N_2 \quad (3.9)$$

where θ and φ are the polar angles; N_1 and N_2 are the uniform random numbers between 0 and 1.

The electrons are followed from the source and through whole history of collisions until they escape limitations. The sequence is continuously repeated for the initial electrons and important parameters are an average of all electrons.

3.4 IMHDMC Numerical Modelling

Plasmas are a kind of ionized gases and consist of electrons, ions and neutral species. In the IMHDMC model, we consider electrons, e^- ; argon ions, Ar^+ ; argon atoms, Ar^0 ; together with basic plasma processes. The two simulation parts are described: the MHD model and MC models. There are three divisions in the MC models: the Ar^+ , Ar^0 and e^- MC models. The more details are described in **Section 3.4.1** and **Section 3.4.2**.

3.4.1 Species and Models in IMHDMC Method

The three species are assumed to be present and described in the IMHDMC model: fast and slow e^- , Ar^+ and Ar^0 . **Table 3-3** shows an overview of types of species and models. The cross sections for elastic (Ar^+/Ar^0), excitation and ionization (e^- and Ar^0) are presented in **Figure 3-11**, where the line 1 represents the elastic cross sections and the line 2 and line 3 represent the excitation and ionization cross sections.

Table 3-3: Type of Species and Models in IMHDMC Method

Plasma species				
Model	Fast e^-	Slow e^-	Ar^+	Ar^0
	MC model	MHD model	MC model	MC model

www.lxcat.net
02 Oct 2015

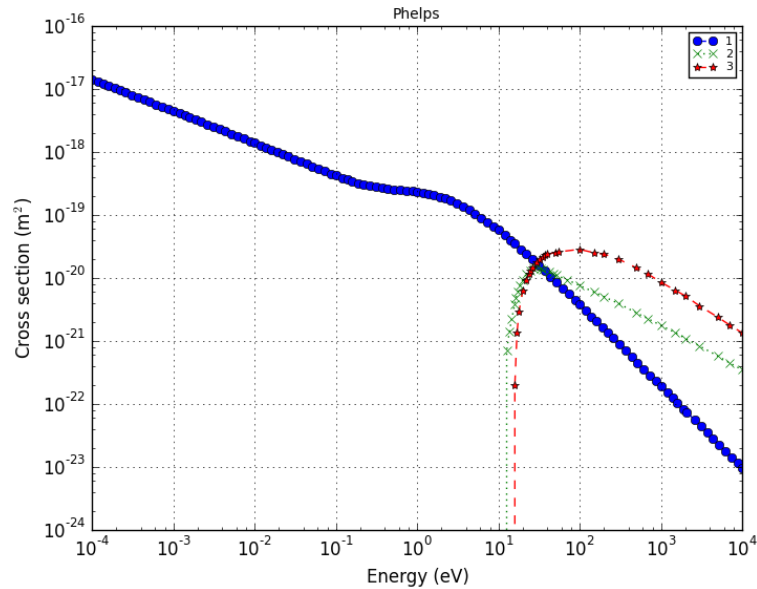


Figure 3-11: Cross Sections for Elastic Process (Ar^+/Ar), Excitation and Ionization (e^- and Ar) Processes in Phelps Database^[43]

3.4.2 IMHDMC Algorithm

In **Figure 3-12**, when a voltage is applied between the electrodes, argon gases start to break down into e^- and Ar^+ and a high current flows through the discharge. The Ar^+ can cause secondary electron emission at the cathode and the emitted electrons lead to more collisions in a plasma during excitation and ionization.

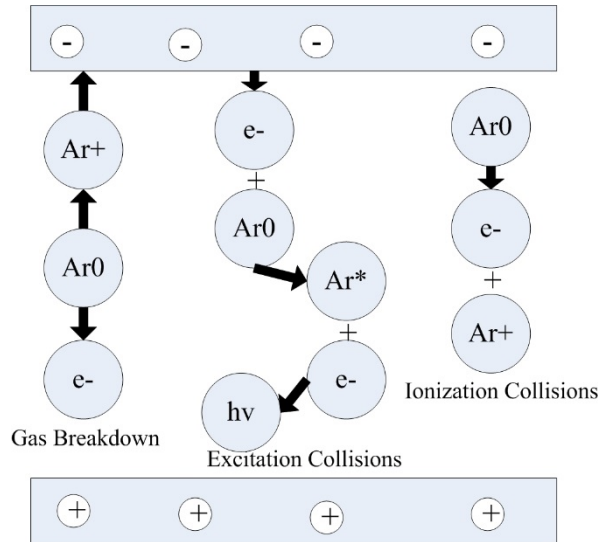


Figure 3-12: Basic Plasma Processes in IMHDMC Model^[44]

The IMHDMC model^[45] has a cylindrically symmetrical geometry, which permits MHD calculations to be performed in the 2D: axial and radial direction, and the MC simulations are calculated in the 3D. The general input includes cell geometry, pressure, temperature, voltage, cross sections and transport coefficients. In the **Figure 3-3**, the MHD model starts to simulate using arbitrary production and loss rates for the three species. This MHD model first gives us approximations of electric field distribution and the Ar^+ flux at the cathode, which are used as input in MC models:

1. The Ar^+ MC model is run using the output from the MHD model. The output includes Ar^+ flux energy distribution at the cathode and production of Ar^0 and e^- .
2. The Ar^0 MC model is simulated and the input is creation of Ar^0 from the Ar^+ MC model. The output is Ar^0 flux energy distribution at the cathode and creation of Ar^+ and e^- .
3. The e^- MC model is run using the electric field distribution and the flux energy distribution of Ar^+ and Ar^0 from the first two steps. The e^- MC model calculates electron flux at the cathode and e^- creation from the Ar^+ and Ar^0 ionization. The output also includes creation of Ar^+ to be used in the Ar^+ MC model and the MHD model.

The three MC models are repeated so that we have the creation of all species until convergence is reached, which is defined by the Ar^+ and Ar^0 flux arriving at the cathode. When the convergence is reached within the three MC models, the MHD model is

calculated again using appropriate production and loss rates from the MC models. This produces new electric field distribution and Ar^+ flux, and these new data are then inserted in the three MC models. Running the three MC models are consecutively repeated in the same way until final convergence is reached.

4 Chapter 4: High-Current Plasma Beams

Simulation and Verification

From **Section 4.1** to **Section 4.3**, we depict the simulations of high-current plasma beams based on the MHD, MC and IMHDMC models. In **Section 4.4**, the experimental verification part gives us a quantitative and qualitative verification for the three methods.

4.1 MHD Simulation Results

The ANSYS FLUENT MHD module allows us to analyze the behavior of electrical conducting fluid flow under the influence of constant electromagnetic fields. The externally-imposed magnetic fields are generated and the MHD simulations are achieved by solving the conservation equations, Ohm's law, Faraday's law and Ampere's law.

4.1.1 Simulation Parameters

1. Mesh Generation

The first step in the FVM is to divide the computational domain into a number of non-overlapping control volumes enclosing each grid point. In this thesis, the software Gambit 2.4.6 is employed to generate the structured non-uniform grid network, as shown in **Figure 4-1**. The prepared grid mesh is then imported into the ANSYS FLUENT in order to solve the set of equations (full discussion is in **Section 3.2.2**).

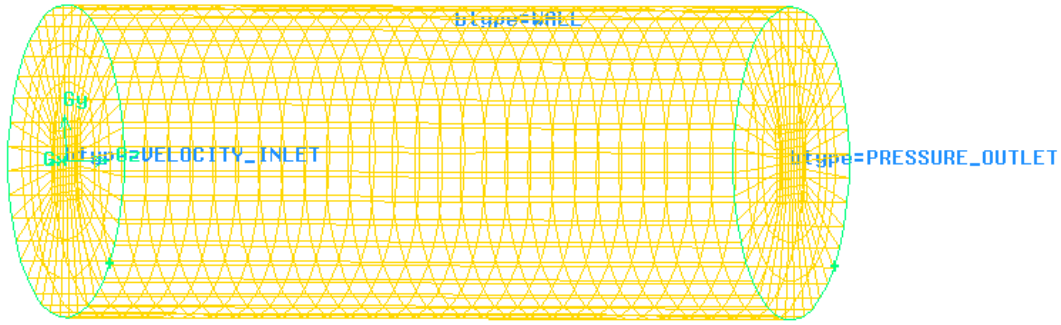


Figure 4-1: Mesh Grids by Gambit for High-current Plasma Beam

When we use the Examine Mesh command button to display an existing mesh and to customize the characteristics of the mesh display. The EquiAngle Skew (Q_{EAS}) is a normalized measure of skewness. In **Table 4-1**, we see that high-quality meshes contain elements that possess average Q_{EAS} values of 0.4 (3D).

Table 4-1: Overall Relationship between Q_{EAS} and Element Quality

Q_{EAS}	Quality
$Q_{EAS}=0$	Equilateral (Perfect)
$0 < Q_{EAS} \leq 0.25$	Excellent
$0.25 < Q_{EAS} \leq 0.5$	Good
$0.5 < Q_{EAS} \leq 0.75$	Fair
$0.75 < Q_{EAS} \leq 0.9$	Poor
$0.9 < Q_{EAS} \leq 1$	Very Poor
$Q_{EAS}=1$	Degenerate

In **Figure 4-2**, Q_{EAS} (0~0.25) in the part (a) has 89.09% active elements, which means that the meshes have an excellent quality; Q_{EAS} (0.25~0.5) in the part (b) has 8.84% active elements, which means that the meshes have a good quality; and Q_{EAS} (0.5~0.75) in the part (c) has 2.07% active elements, which means that the meshes have a fair quality. Therefore, we can identify that the MHD model meshes have a high equality.

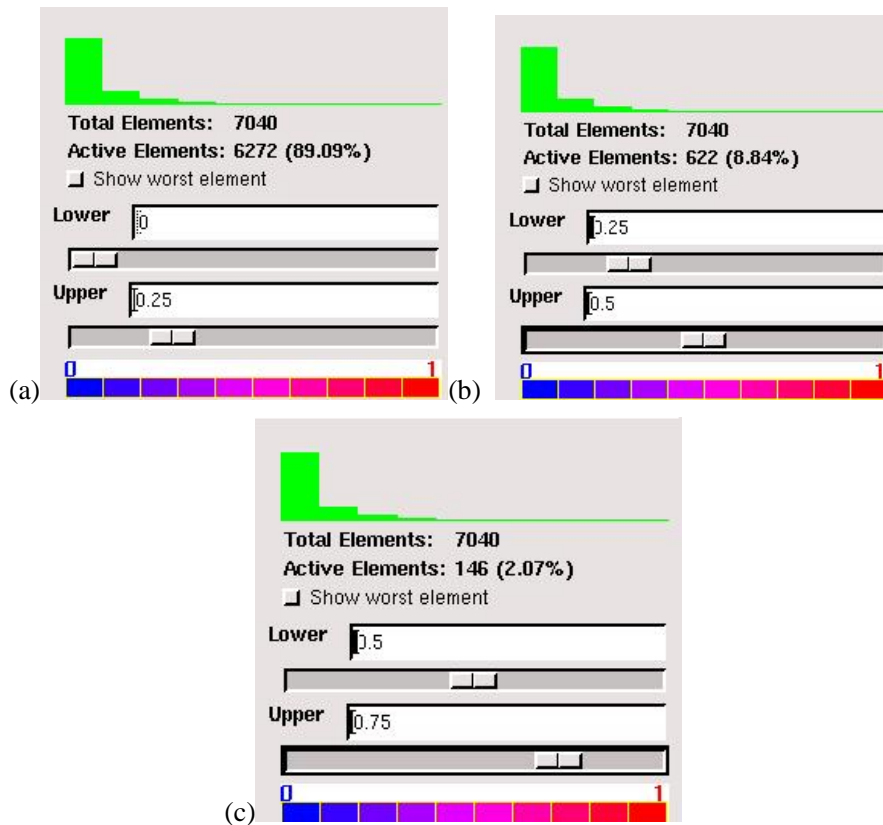


Figure 4-2: Mesh Examination by Range Option and EquiAngle Skew Quality Type

In **Figure 4-3**, Gambit shows the 3D mesh display by sphere option display type and EquiAngle skew quality type in four quadrants. It displays a region of the mesh defined with respect to the cutting plane and the elements exist above the cutting plane.

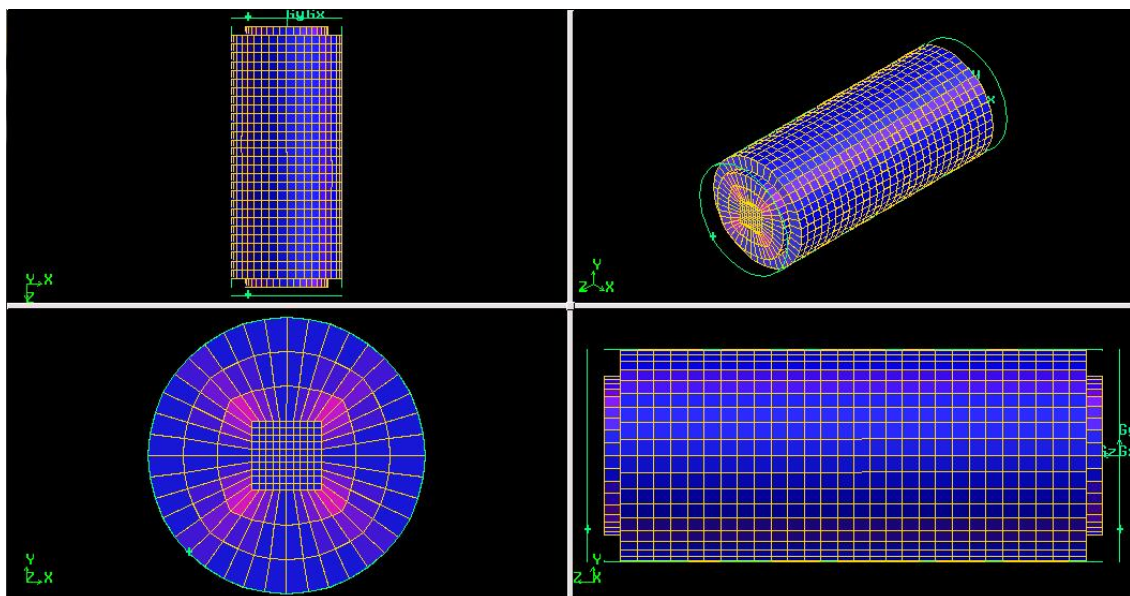


Figure 4-3: 3D Mesh Examination by Sphere Option Display Type and EquiAngle Skew Quality Type

2. Pressure-based Solver with Segregated Algorithm

The ANSYS FLUENT has both pressure-based and density-based solvers. Originally, the pressure-based approach was developed for low speed incompressible flows, while the density-based approach was mainly used for high-speed compressible flows^[46]. However, both the two solvers depend on the Mach number^[47], M :

$$M = \frac{v}{c_s} \quad (4.1)$$

where c_s is the speed of sound in a plasma ($379.16 \times 10^3 \text{m/s}$).

The high-current plasma beams are regarded as subsonic flow since the M is equal to 3×10^{-6} . In **Figure 4-4**, the pressure-based solver algorithms are illustrated: segregated algorithm and coupled algorithm.

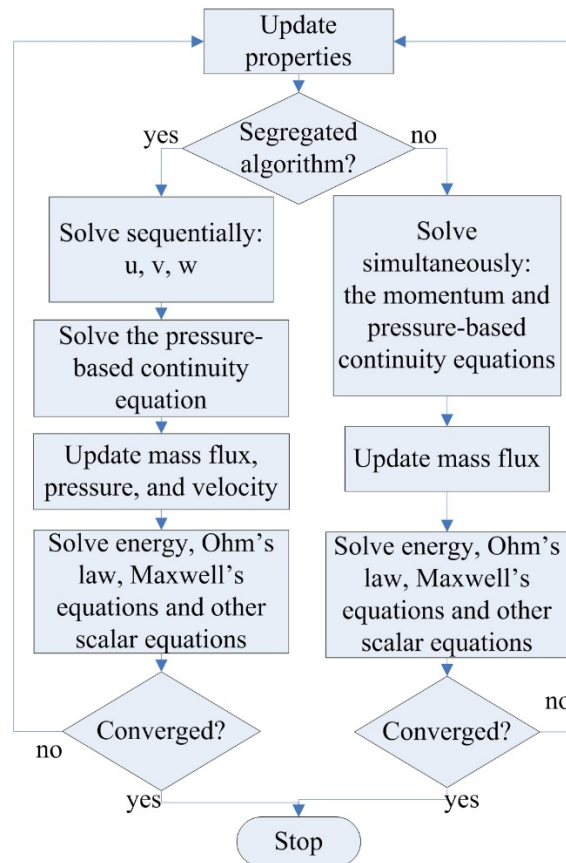


Figure 4-4: Overview of Pressure-based Algorithms^[48]

In this study, the pressure-based solver with the segregated algorithm is used and the governing equations are solved sequentially^[49]. Because the governing equations are

non-linear and coupled to one another, the solution loop is iteratively conducted until solution converges.

3. Spatial Discretization

The values are required from **Equation 3.2** to **Equation 3.4** in the spatial discretization, which is conducted using the upwind scheme. The upwind scheme means that we determine the value of MHD model from the cell values in the two cells upstream of the face relative to the flow direction. In **Figure 4-5**, the second-order upwind scheme is used for discretization of density in the mass equation, face pressure in the momentum equation because of its combination of accuracy and stability.

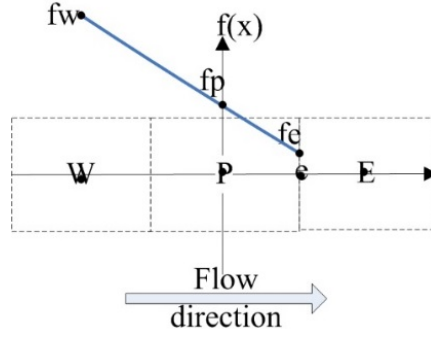


Figure 4-5: Second-order Upwind Scheme

$$\frac{f_e - f_p}{x_e - x_p} = \frac{f_p - f_w}{x_p - x_w} \quad (4.2)$$

$$f_e = \frac{(f_p - f_w)(x_e - x_p)}{x_p - x_w} + f_p \quad (4.3)$$

To interpolate f_e value, the scheme assumes that the gradient between the cell W and the surface with center point P is same as that between the cell E and the surface with center point P. Using **Equation 4.2** and **Equation 4.3**, we obtain the value of f_e . For **Equation 3.5** and **Equation 3.6**, the magnetic field and current density are evaluated based on a standard linear interpolation of the adjacent node values.

4. Under-relaxation Schemes

It is a good practice to begin a calculation using the default under-relaxation factors. When the under-relaxation factor with too large value can lead to oscillatory or even divergent iterative solutions. By contrast, a value which is too small can cause extremely slow convergence. The under-relaxation factors for the equations in **Section**

3.2.2 are set to 0.8~0.9. As some additional source terms are added to the momentum and energy equations, the under-relaxation factors for these equations are reduced to improve the rate of convergence.

5. Convergence Criteria

When evaluating whether convergence has been reached, there are the three indicators: (a) residuals have decreased to a sufficient degree, (b) solution no longer changes with more iterations and (c) overall mass, momentum, energy and scalar balances are obtained. A sensitivity analysis is recommended: (a) comparing the solutions for various convergence values and (b) choosing the minimum value after no changes are observed in the solutions.

In the MHD model, the turbulent flow with Reynolds number ($Re > 4000$) and the standard $k-\epsilon$ model with the standard wall functions are used. In **Table 4-2**, the material properties and relevant constants are applied.

Table 4-2: Physical Argon Properties in MHD Simulation^[50]

Density (kg/m ³)	Dynamic viscosity (kg/m-s)	Electric conductivity (S/m)	Thermal conductivity (W/m-K)	Magnetic permeability (H/m)
1.62	0.00002125	1000000	2.5	0.01257

4.1.2 MHD Simulations

4.1.2.1 2D Simulation Results

1. Convergence

Figure 4-6 exhibits a minimum convergence history with the residuals, which are smaller than 0.01, for a steady-state run in the MHD model. The X-axis means the number of iterations and Y-axis represents the residuals of continuity, velocity (v_x, v_y, v_z), K-epsilon model. Each variable is in different color, as shown in the legend, so that it is easy to obtain the corresponding residual for each variable.

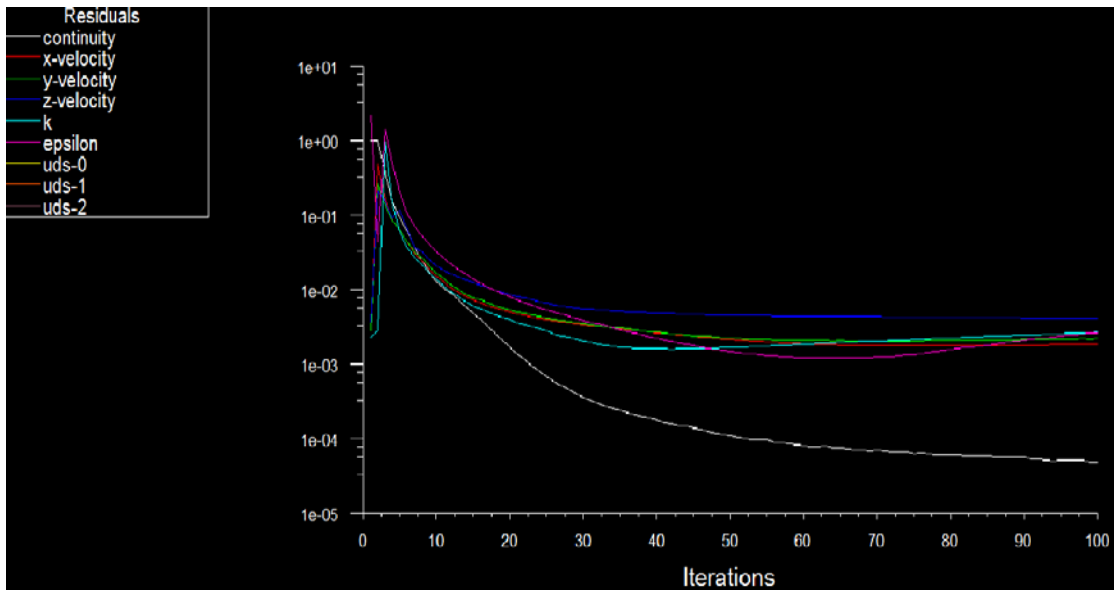


Figure 4-6: Convergence History of High-current Plasma Beam

2. Static Pressure

Energy and mass transfer processes are closely coupled in high-current plasma beams and a static pressure distribution therefore need to be understood. **Figure 4-7** shows the static pressure distribution of outlet in the radial direction at the XY cross section, where the X-axis denotes the radial position in plasma beam and the Y-axis denotes the static pressure. The static pressure consists of two pressure circles, which are similar in size and continually change. The condition for emergence of two pressure circles, which is equivalent to the condition that the vortex current flow^[51] occurs in the same way. The phenomena is due to the non-uniformity of the argon transport coefficients in the high-current plasma beams.

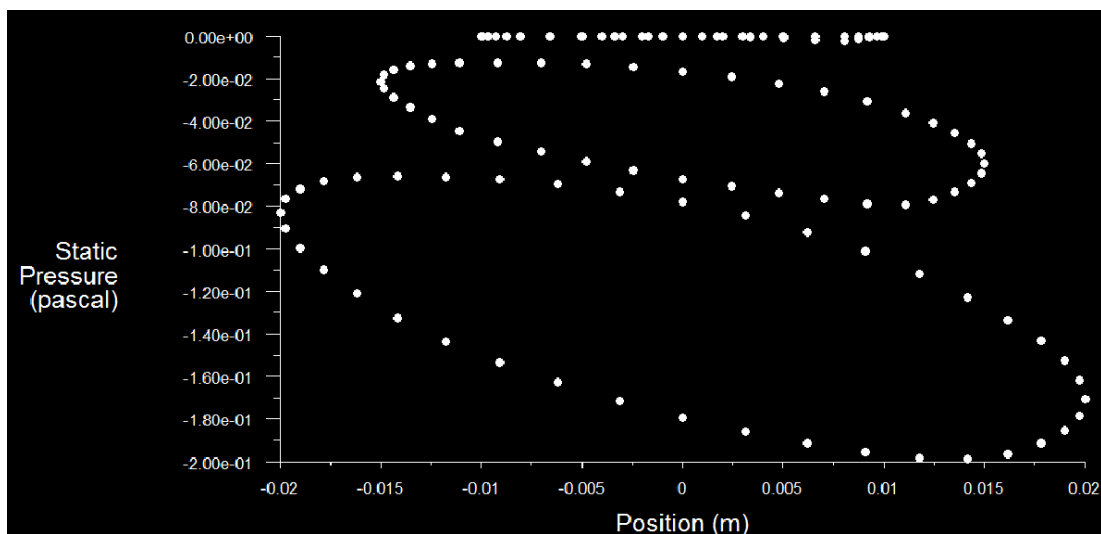


Figure 4-7: Static Pressure Distribution of Outlet in Radial Direction

3. Velocity Monitor

The initial velocity at the inlet is set to be $v_x=0$, $v_y=0$ and $v_z=1.2\text{m/s}$. In order to monitor the trend of velocity, the velocity monitor is put at the outlet based on mass weighted average. **Figure 4-8** shows the mass weighted average for velocity at the outlet, where the X-axis means the number of iterations and the Y-axis means the mass weighted average for velocity at the outlet. The outlet velocity firstly drops so fast, after 200 iterations, the mass weighted average for velocity becomes stable and close to 0.

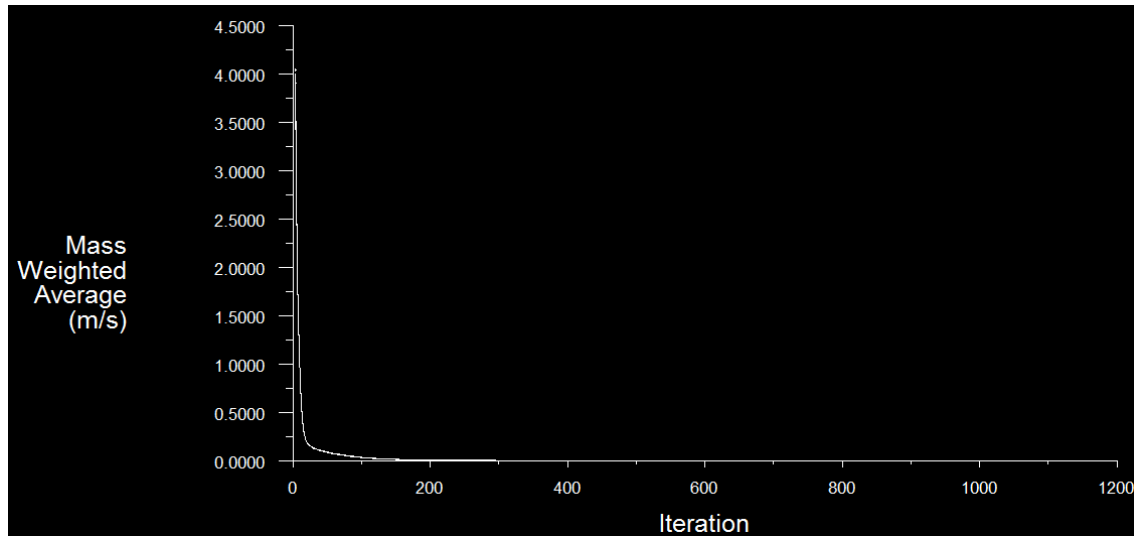


Figure 4-8: Mass Weighted Average for Velocity at Outlet

It is useful to obtain information about the velocity magnitude distribution in the radial direction in **Figure 4-9**, where the X-axis is the radial position in plasma beam and Y-axis is the velocity magnitude. The velocity magnitude distribution is similar to a Gaussian distribution so that we can identify that the further the distance of the central axis, the smaller the value of the velocity magnitude. The largest velocity magnitude is around 0.7 m/s and the smallest velocity magnitude is around 0.2 m/s. At the $\pm 0.006\text{m}$ positions, the velocity quickly drops; after that, it becomes stable.

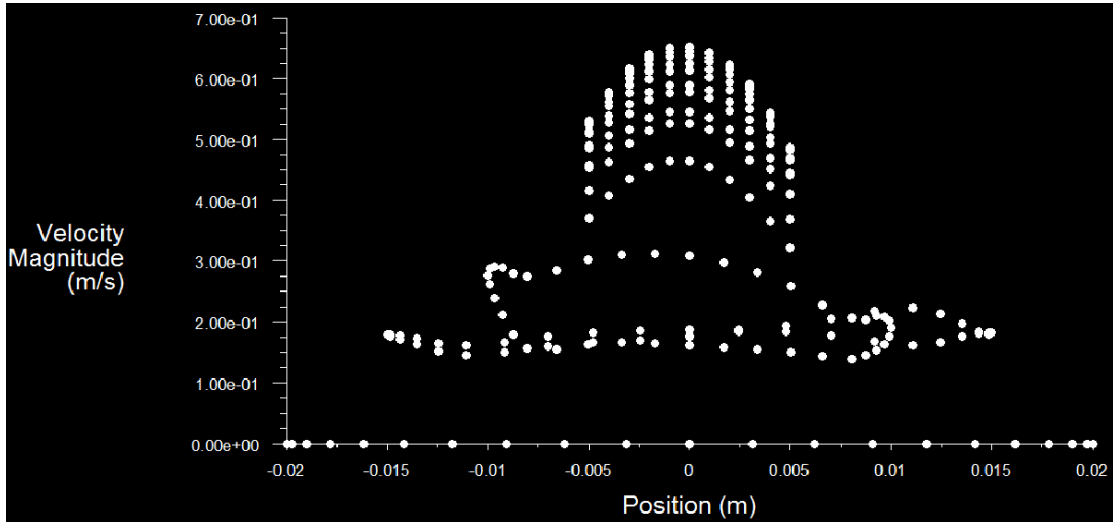


Figure 4-9: Velocity Magnitude of Outlet in Radial Direction

4.1.2.2 3D Simulation Results

1. Contour

In **Figure 4-10**, it is concluded that the density of the high-current plasma beams is not uniform due to non-uniform transport coefficients, and the density changes around 1.62kg/m^3 .

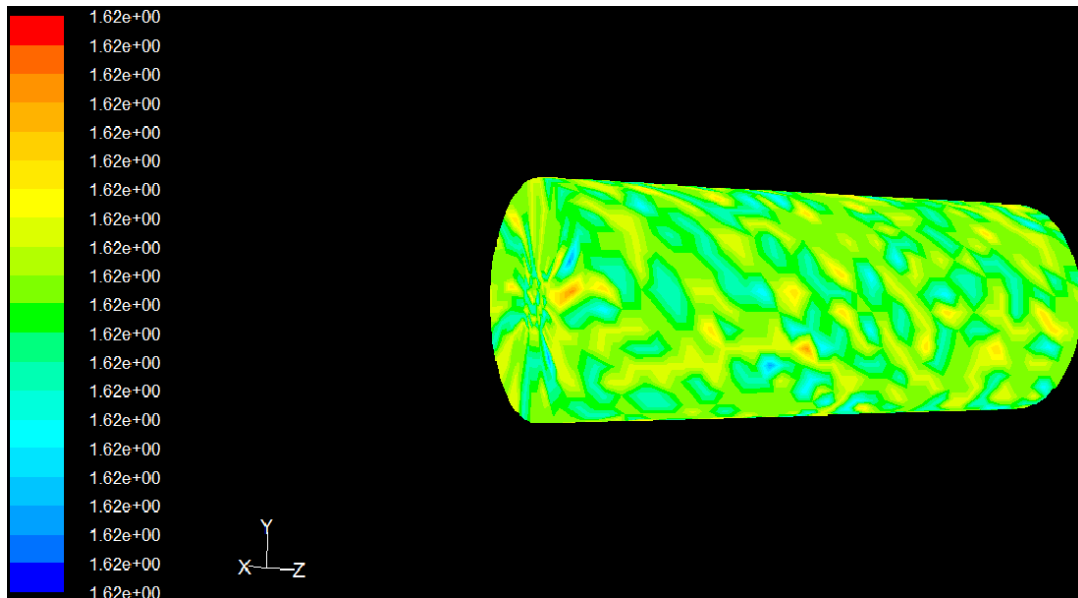


Figure 4-10: 3D Density Distribution of High-Current Plasma Beam

2. Vector

In **Figure 4-11**, due to the external applied magnetic fields ($B_{0x}=0.5\text{T}$, $B_{0y}=0.5\text{T}$, $B_{0z}=1\text{T}$), they give a helical shape of magnetic field. The Lorentz force is produced in

the three directions so that the velocity vector has the different magnitudes and directions. When the velocity vector is close to the inlet, it changes to the opposite direction at the edge of the MHD model. Near the conducting wall, the velocity vector rotates along the Z direction. At the inner MHD model, it rotates at a higher speed than at the edge.

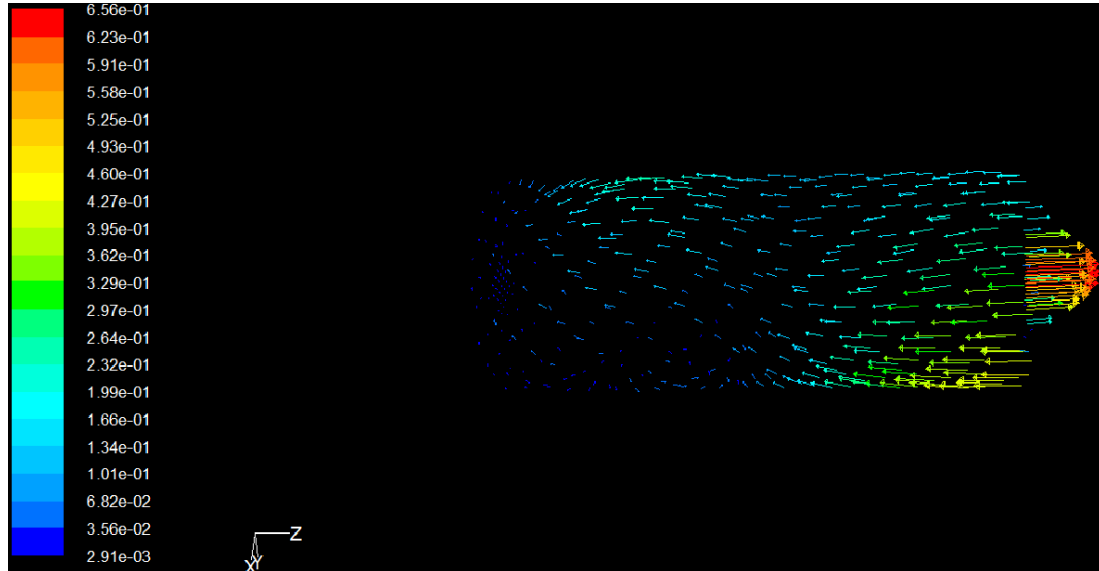


Figure 4-11: 3D Velocity Vector of High-Current Plasma Beam

4.2 MC Simulation Results

The simulations of an e-beam source in the electromagnetic fields are illustrated, where the electric fields are uniform and the magnetic fields are produced by a quadrupole. It is critical to choose a sufficient number of iterations to score accurate results. In this thesis, the number of initial electrons is 1,000,000, which limits the relative fluctuation within 1%. The computations are run on the Dell INSPIRTION-PC with a 2.5 GHz Intel core i5-2450M processor and the computation time varies from 30 minutes to five hours.

4.2.1 Simulation Instruments

4.2.1.1 Notepad++

Notepad++ is a free source code editor as shown in **Figure 4-12**. Running in the

Windows environment, Notepad++ is written in C++ and uses the pure Win32 Application Programming Interface (API) and the Standard Template Library (STL) which ensures a high execution speed and small program size.

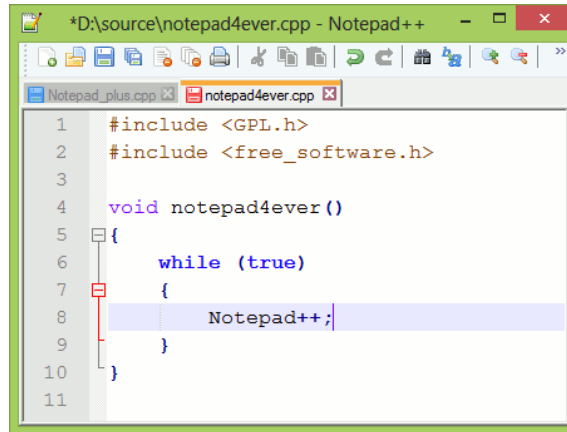


Figure 4-12: Notepad++ Programming Interface

4.2.1.2 PHITS 2.64

The multi-purpose Monte Carlo Particle and Heavy Ion Transport code System (PHITS)^{[52][53]} based on the NMTC (Nuclear Meson Transport Code) and JAM (Jet-Aa Microscopic Transport Model)^[54] has been developed. The physical processes which PHITS includes are divided into the two categories, as shown in **Figure 4-13**: transport processes and collisions. In the transport processes, the PHITS can simulate particle motion under external fields, such as magnetic and electric fields. Without external fields, neutral particles move along a straight trajectory with constant energy until a next collision. The second category is collisions. According to mean free path, the PHITS chooses next collision point using the MC method. To generate secondary particles of collisions, we need the information on final state of the collisions.

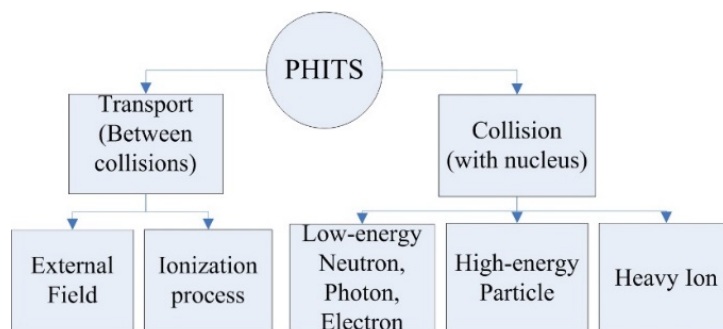


Figure 4-13: Particle Transport Processes and Collisions in PHITS

4.2.1.3 Assisted Tools

In the MC simulations, we also use assisted tools to program and display the high-current plasma beams. In **Table 4-3**, the names, types and function are simply described.

Table 4-3: Assisted Tools in MC Simulations

Name	Type	Function
ANGEL	Programming language	ANGEL is used to draw fine graphs and creates EPS ^a files from input. It is a translator from ANGEL language to PostScript (PS) language, which interprets commands and data and creates PS files.
GSview 5.0	Graphical interface	GSview is used to display image files created by the PHITS, which are written in the EPS format.

^aEPS denotes the Encapsulated PostScript.

4.2.2 MC Simulation Steps

The source code of the PHITS is written in Fortran (Formula Translating System) and the MC simulation flowchart is shown in **Figure 4-14**. We first specify the geometry of 3D virtual space and the information of source particles. Next, we tally various quantities by simulating electrons.

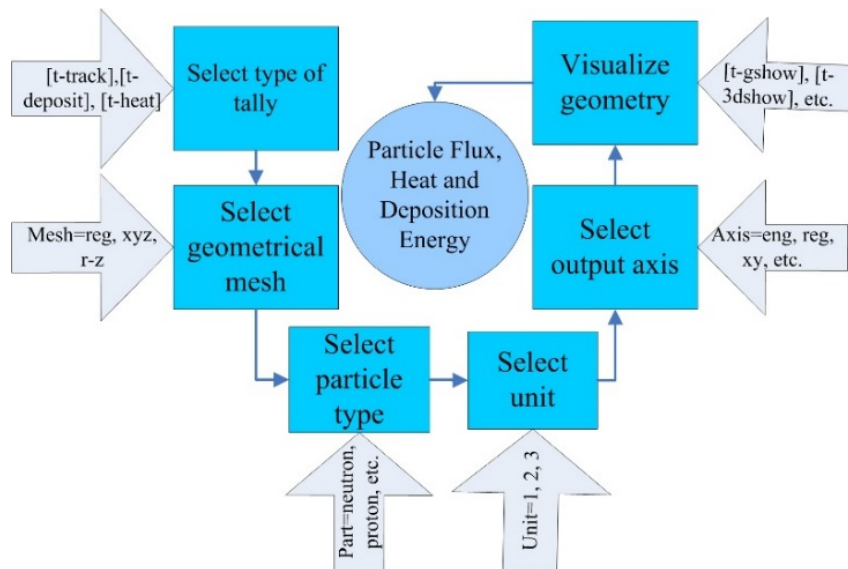


Figure 4-14: Flowchart of MC Simulation

1. Geometry and Material

The geometry of the high-current plasma beams is defined by the Boolean operators including cell and surface definitions. We use infinite space and fill cells with certain

materials or void: the wall (cell 101) is filled with copper, the cell 100 is filled with argon gas and the cell 102 is void. The properties of argon gas and copper are listed in **Table 4-4**.

Table 4-4: Argon Gas and Copper Properties in MC Simulations

	Argon	Copper
Radius (cm)	2	2 (ID ^a)/2.5 (OD ^b)
Length (cm)	10	10
Density(g/cm ³)	1.62e-3	8978
Initial electron projectile energy (MeV)	0.158	0

^a ID denotes the inner dimension.

^b OD denotes the outer dimension.

2. Source

We select a cylindrical shape of source distribution with mono-energy source particles. The radius of the cylindrical source is 2cm and the length is 10cm. The total number of electron source particles is 1000,000, since in the calculation of statistical uncertainties, the history variance mode is selected, which calculate the standard deviations using variances between tally results of each history. The standard deviation depends only on the total history number so that relative errors are proportional to the number of history, which is equal to the number of electron source particles. They go through the cell 100 along the Z-axis. During this process, it produces other particles, such as neutrons and photons.

3. Tally

We use tallies [t-3dshow] and [t-gshow] to check geometries of the MC model, such as the 2D and 3D visualizations. Besides, we use tallies [t-track], [t-heat] and [t-deposit] to calculate physical quantities, such as particle flux, heat and deposit energy.

4. Control

Some control functions are available for us to improve the MC simulation accuracy, such as calculation mode (icntl=0~12), particle transport simulations and physical models. We can also obtain better statistics by increasing the history number.

4.2.3 MC Simulations

4.2.3.1 Geometry of MC Model

The tally [t-3dshow] gives us the 3D plasma beam geometry, as shown in **Figure 4-15**.

It is obvious that the argon gas is red and the copper is cyan.

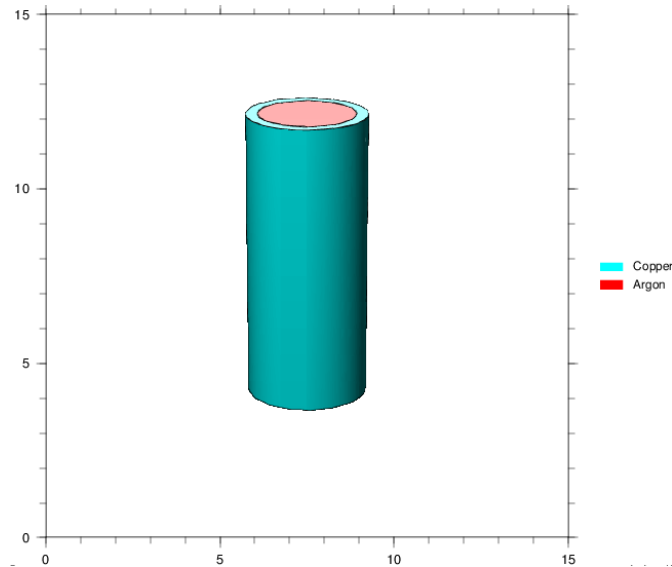


Figure 4-15: 3D MC Model by Tally [t-3dshow]

In **Figure 4-16**, we check the 2D geometry of the MC model by the tally [t-gshow].

Since the sphere (cell 102) is hypothetical, it is assumed to be void.

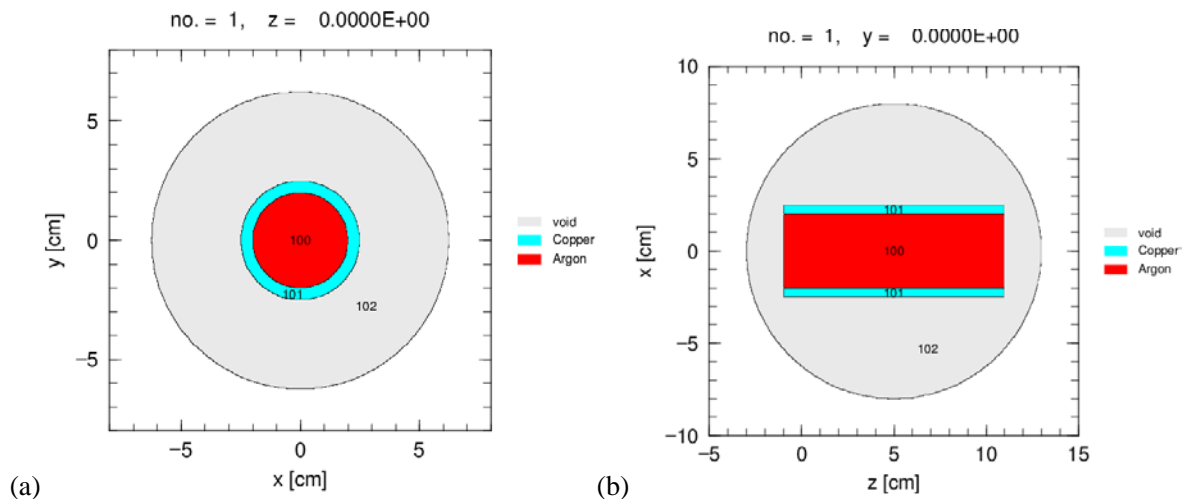


Figure 4-16: 2D MC Model by Tally [t-gshow] on (a) XY Plane and (b) XZ Plane.

4.2.3.2 Amount of Particles

The tally [t-product] tallies source particles, particles and nuclei produced by nuclear reaction and decay and its unit is [1/source]. In **Figure 4-17 (a)**, the amount of all particles is shown on the XZ plane and its relative errors are shown in **Figure 4-17 (b)**. Warm colors indicate that relative standard errors are large (close to 1), while cold colors represent small relative standard errors. The source particles are generated in the cell 100 and they also transport to the cell 101. In the center of the plasma beams, the number of all particles is the most and it is equal to 10^{-3} [1/source] \times 1000000[source]=1000. At the edge of the plasma beams, the number of all particles becomes small and it is smaller than 10^{-5} [1/source] \times 1000000[source]=10. From the relative error distribution, it is obvious that it is close to 0.01.

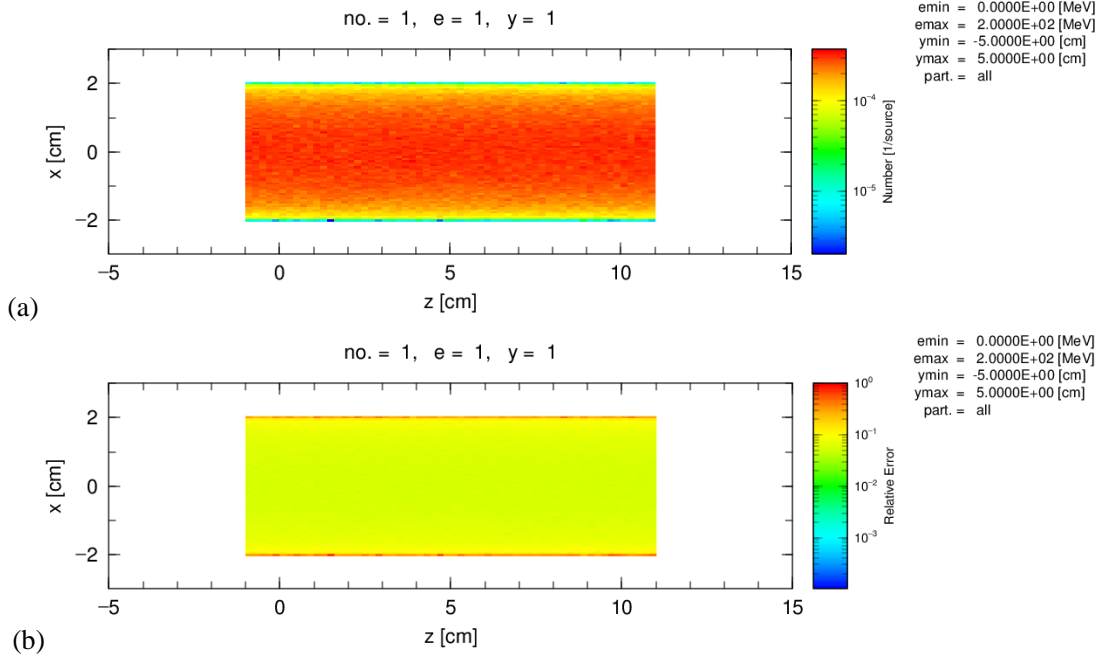


Figure 4-17: (a) Amount of Particles by Tally [t-product] and (b) The Relative Errors

In order to obtain statistical uncertainties, we calculate standard deviations using variances between tally results of each batch and history. The standard deviation σ_d is calculated by

$$\sigma_d = \sqrt{\frac{\sum_{i=1}^N (x_i w_i / \bar{w})^2 - N \bar{x}^2}{N(N-1)}} \quad (4.4)$$

where N is the total history number (istdev=2), x_i and w_i are the tally results and the source weight of each sample, respectively. Therefore, \bar{x} and \bar{w} are the mean values of the tally results and the source weights of N samples. The ratio of σ to \bar{x} is written as the relative error in tally output files.

4.2.3.3 Electron Flux

We check electron flux of all regions in magnetic fields by tally [t-track] and set icntl=5. In **Figure 4-18 (a)** and **(b)**, the default of the electron initial energy is from 0 MeV to 10^{-2} MeV. In the argon gas region (cell 100), the flux of electron is 10^{-3} [1/cm²/ source]. The relative errors ($\approx 10^{-2}$) are low and it is proved that the electron flux is accurate. In the copper wall (cell 101), the electron flux is 10^{-4} [1/cm²/ source]. However, its relative errors are close to 1, the electron flux is not accurate so that it should be reasonably neglected.

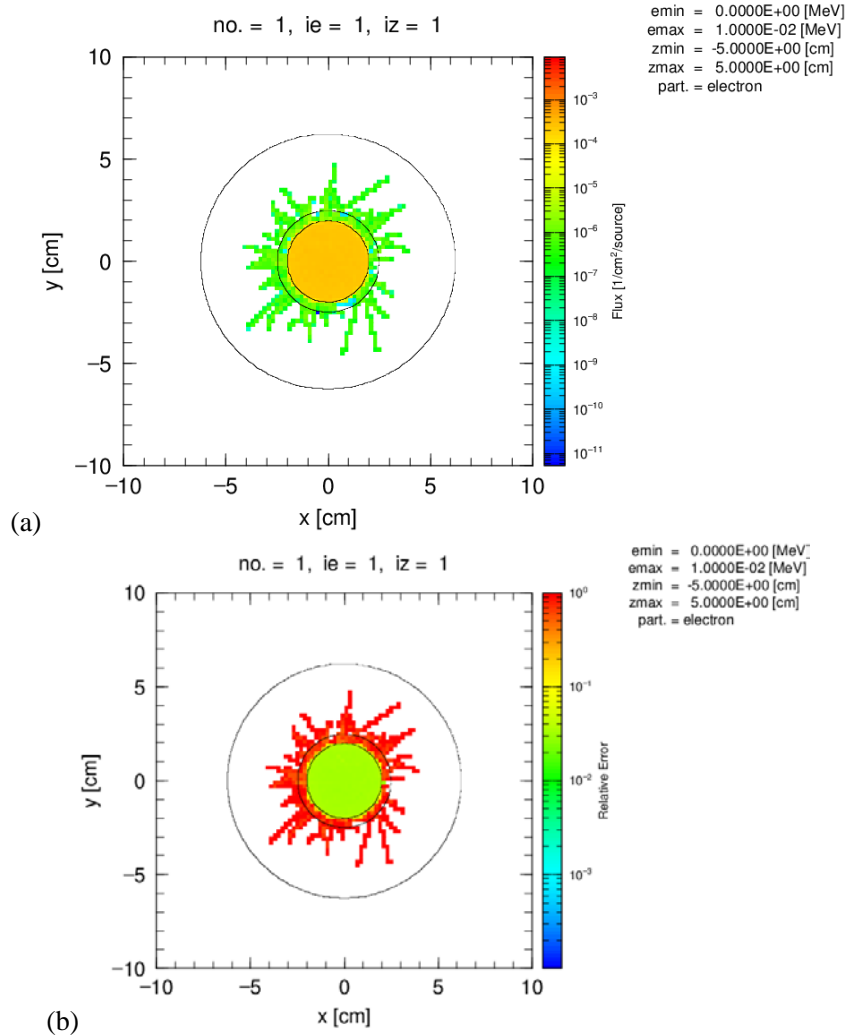


Figure 4-18: (a) Electron Flux by Tally [t-track] on XY plane and (b) The Relative Errors. Similarly, under the effect of magnetic fields (10 KG), the electron flux on the XZ plane is shown in **Figure 4-19 (a)**. The average electron flux is close to 10^{-2} [$1/\text{cm}^2/\text{source}$] in the argon gas region. In the cathode (left) part, the electron flux are increased from 10^{-6} [$1/\text{cm}^2/\text{source}$] to 10^{-3} [$1/\text{cm}^2/\text{source}$]. The electron flux in the cell 102 symmetrically distributes along the X-axis. Additionally, the inner region has the highest value and the outward region has the lowest value. In the anode (right) part, the electron flux is higher than that in the cathode part and its electron flux range is from 10^{-4} [$1/\text{cm}^2/\text{source}$] to 10^{-2} [$1/\text{cm}^2/\text{source}$]. The level line of electron flux in the anode is not clearer than that in the cathode. In **Figure 4-19 (b)**, the relative errors are so small in the cells 100 and 102, so that it is convinced that the simulation results have high accuracy. In order to finish these MC simulations, it takes 1 hour to run the [t-track] algorithm.

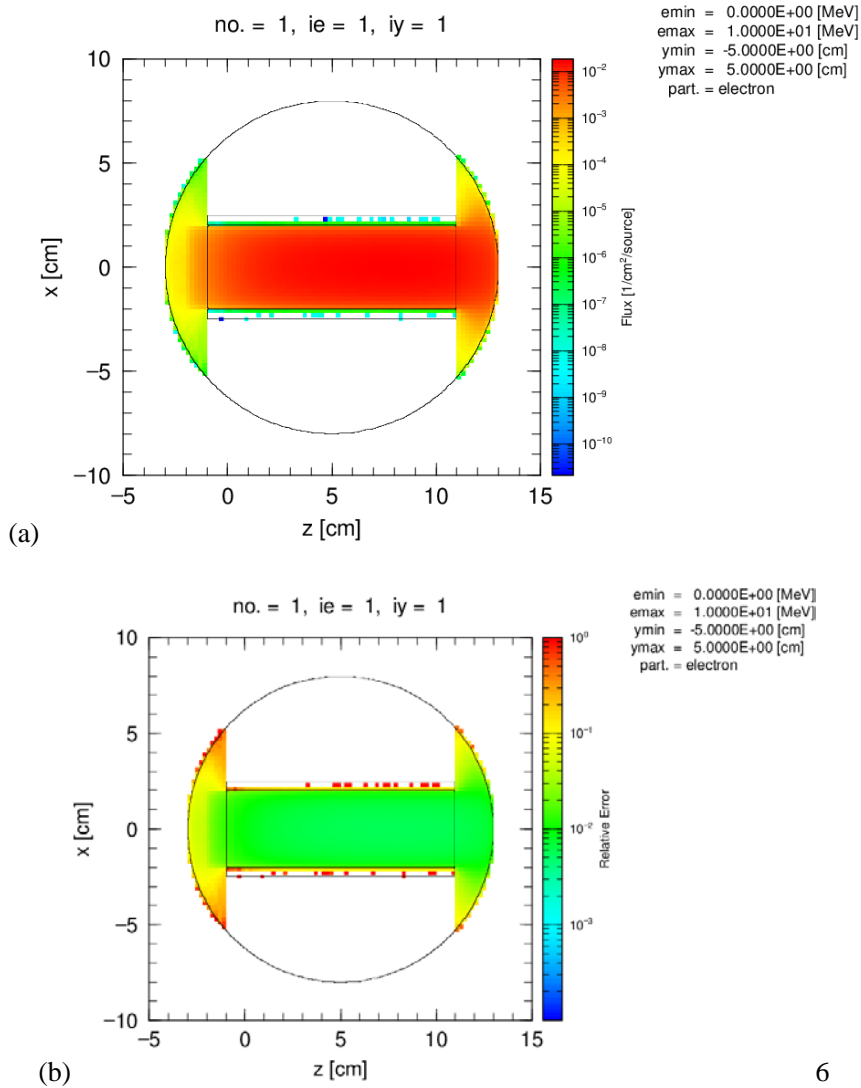


Figure 4-19: (a) Electron Flux by Tally [t-track] on XZ Plane and (b) The Relative Errors

4.2.3.4 Deposit Energy Distribution

Ionization energy losses by charged particles are scored by tally [t-deposit] and its unit is 1/source. Particles with energy below e_{min} parameters are not traced by PHITS simulation. We use reg mesh in the argon gas region, which is a geometrical mesh and divides the regions in cells. The E-type=3 denotes logarithmic interval and the ANGEL parameters (angel= $y_{min}[1E-06]$ $y_{max}[1E-00]$) are used to change layouts of EPS figures. In **Figure 4-20**, the deposit energy distribution has Gaussian distribution. From the 10^{-2} to 10^{-1} MeV, the particles are the most. Since the total number of particles is 1,000,000, more than 10,000 source particles have $10^{-2} \sim 10^{-1}$ MeV energy. With the increases of the

deposit energy from being 10^{-7} MeV, the number of particles are growing.

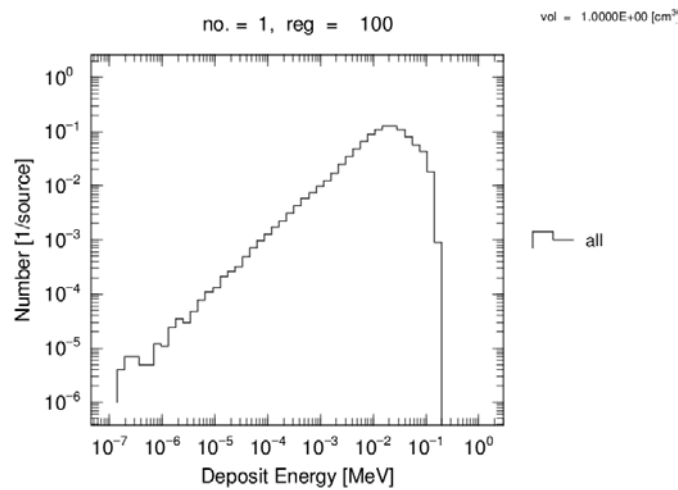


Figure 4-20: Deposit Energy by Tally [t-deposit] in Cell 100

4.2.3.5 Heat Distribution

During the processes of argon gas excitation and ionization, neutrons and photons are produced. We can use tally [t-heat] to calculate neutrons and photons dose by the Kinetic Energy Released per unit Mass (KERMA) approximation. In the thesis, for electron=1 with electron transport, we do not use the KERMA factors of photon, but obtain the heat from the energy loss of electrons. In **Figure 4-21(a)**, the heat in the cathode region is lower than that in the anode region and the value is smaller than 10^{-6} [MeV/source]. The heat is almost uniform except the cathode part. There are still some heat in the cell 101 due to neutrons penetrating into the copper wall. However, the heat is smaller than 10^{-8} [MeV/source]. In **Figure 4-21(b)**, the relative errors of heat are smaller than 0.1 in the cell 100. The relative errors at the edge of copper is not reasonable, which can be optionally neglected. It takes around 1 hour 16 minutes to obtain the heat distribution and its relative errors.

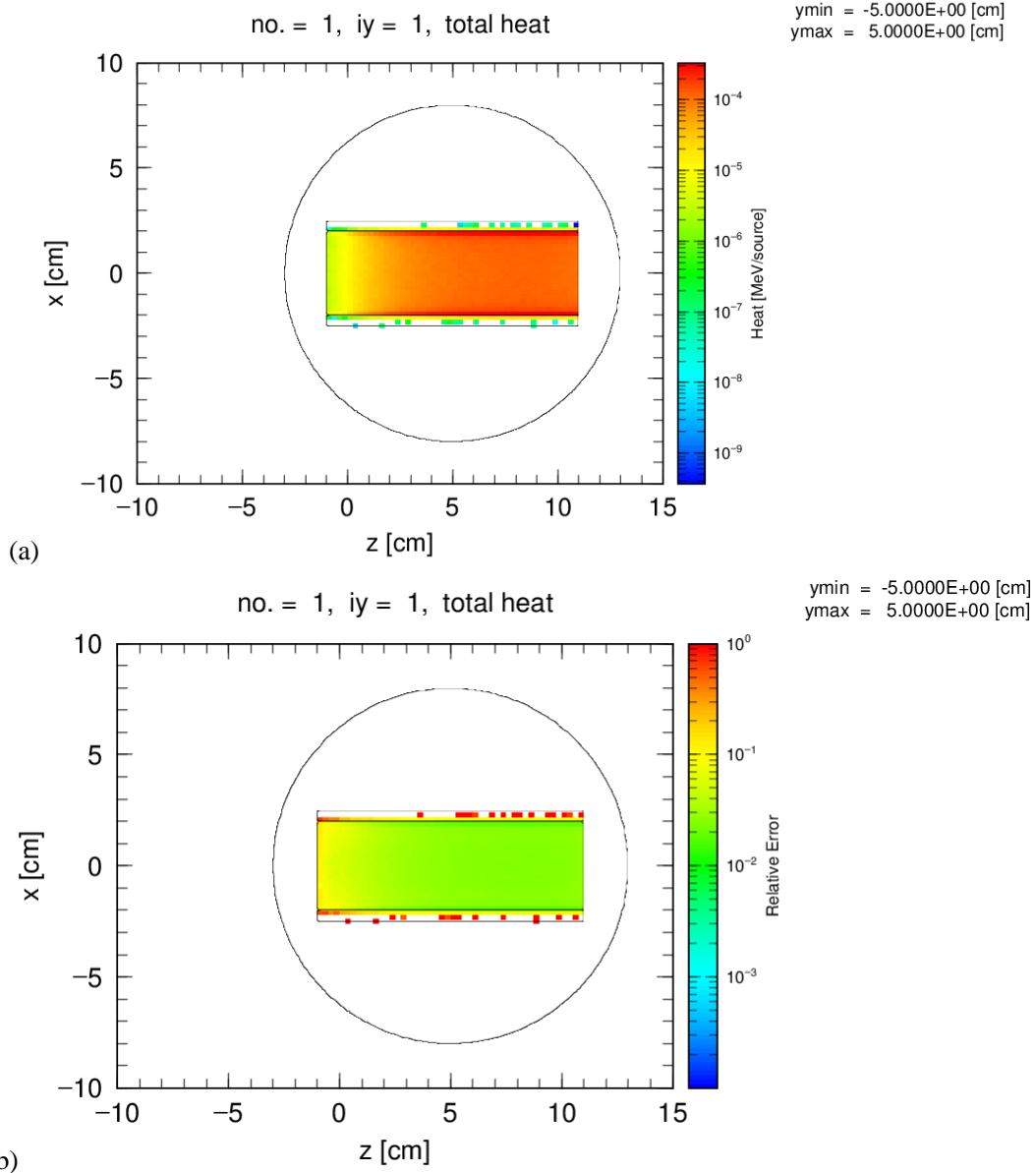


Figure 4-21: (a) Dose of Neutrons and Photons by Tally [t-heat] and (b) The Relative Errors

4.3 IMHDMC Simulation Results

The IMHDMC method is a comprehensive method that integrates the MHD and MC simulation results together. It links the magnetohydrodynamic fluid with the particle transports and collisions in the high-current plasma beams. The MHD simulations define spatial distribution of electric fields and these distribution are then employed by the MC simulations to characterize heat and deposit energy. The Ar^0 are assumed to have a uniform density ($1.65 \times 10^{16} \text{ cm}^{-3}$) at the simulation conditions.

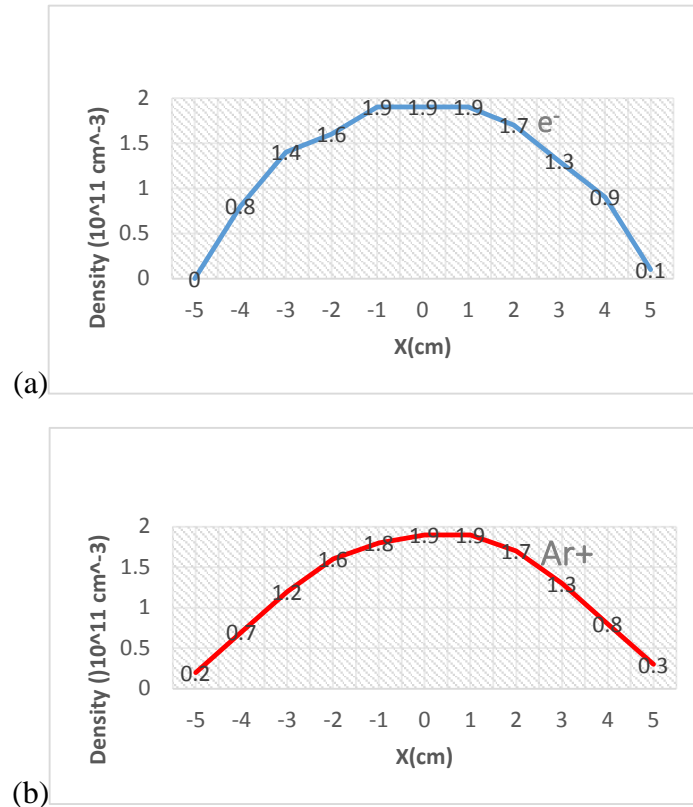


Figure 4-22: 1D Density Profiles of (a) e^- and (b) Ar^+ in IMHDMC Model

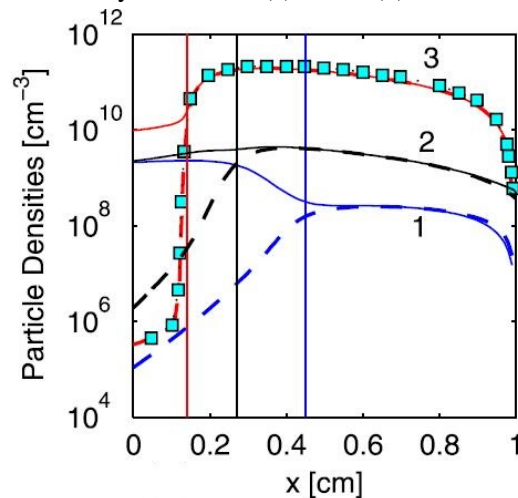


Figure 4-23: Validation of IMHDMC Method by References

In **Figure 4-22(a)** and **(b)**, the electron density is almost same as the Ar^+ density in the high-current plasma beams, where the horizontal axis is the X-axis and the Y-axis is the electron density. In **Figure 4-23**, the line 1 denotes the fluid model, the line 2 denotes the extended fluid model, the line 3 denotes the hybrid model, which is equivalent to the IMHDMC model in the thesis; and the point line denotes the reference^[55] data. The vertical lines in **Figure 4-23**, represent the borders between the

cathode sheath and negative glow regions of the discharge for the different models. Compared to the results, which are the electron and ion densities, in **Figure 4-23**, the simulation results in **Figure 4-22** computed by the IMHDMC model lead to the closer plasma densities.

In **Figure 4-24(a)**, the temperature distribution produced by the IMHDMC method correspond to the MHD and MC simulation results. The ANSYS FLUENT MHD module is used for the MHD simulations, while the PHITS is used for the MC simulations. According to the IMHDMC simulation results in **Figure 4-24(b)**, the Lorentz force is the main parameter which affects the fluid flow in the magnetic fields. In the center of the high-current plasma beams, there is the largest Lorentz force.

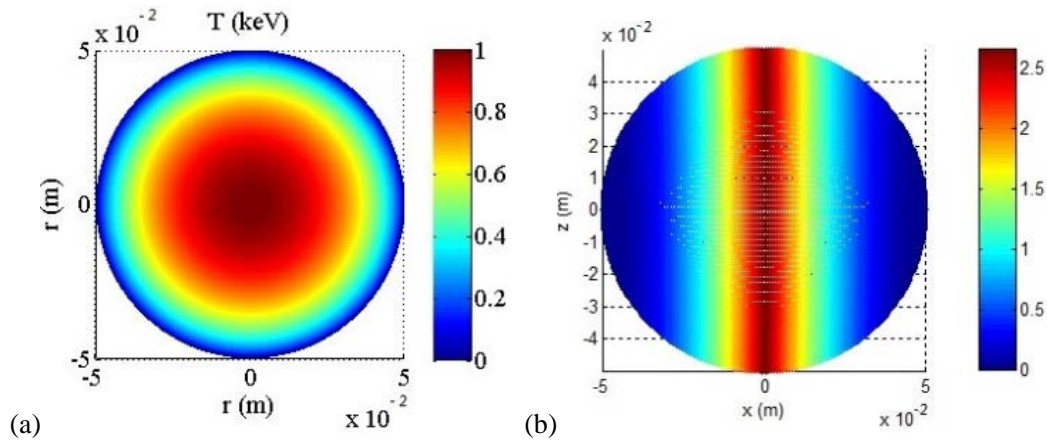


Figure 4-24: (a) Temperature Distribution and (b) The Lorentz force in IMHDMC Model

4.4 Experimental Verification

The main purpose of the HOPE's experiment is to test the formation of a high-current plasma beam, which will be used to guide the construction of an apparatus. The same four plasma beams are arranged into a balanced tetrahedral structure so that all four beams will pass through a central focal point.

4.4.1 Current-Voltage Relation

Current $I(t)$ in an electric circuit is defined as the rate of flow of a charge $Q(t)$ passing through it. Thus the charge on the electrodes is equal to the integral of the current as

well as proportional to the voltage. It is assumed that the initial voltage is equal to zero and there is no resistance through a plasma or wires. This is the integral form of capacitor equation^[56]:

$$V(t) = \frac{Q(t)}{C} = \frac{1}{C} \int_{t_0}^t I(t) dt \quad (4.5)$$

where V is the voltage across the capacitor, Q is the charge stored in the capacitor, C is the capacitance and I is the current.

Taking derivative of **Equation 4.5** and multiplying by C produces the derivative form:

$$I(t) = \frac{dQ(t)}{dt} = C \frac{dV(t)}{dt} \quad (4.6)$$

After obtaining the relationship between a voltage and time, it is easy to calculate a current produced by a DC discharge.

4.4.2 High-Current Plasma Beam Experiment

In **Figure 4-25**, the test setup with capacitors is set at the near-vacuum ambient pressure to produce a DC discharge. The capacitors then discharge an electric current between the electrodes, with transient electromagnetic fields accelerating the resulting plasma. This test setup basically consists of a cylindrical quartz chamber, necked at both ends to accommodate stainless steel end flanges and seals. The electrodes and some instrumentation ports pass through the end flanges. Not shown in the figure is the fueling flow loop and small tank. A vacuum pump can be connected to the fitting on the flange in the foreground. The initial conditions are as follows in **Table 4-5**.

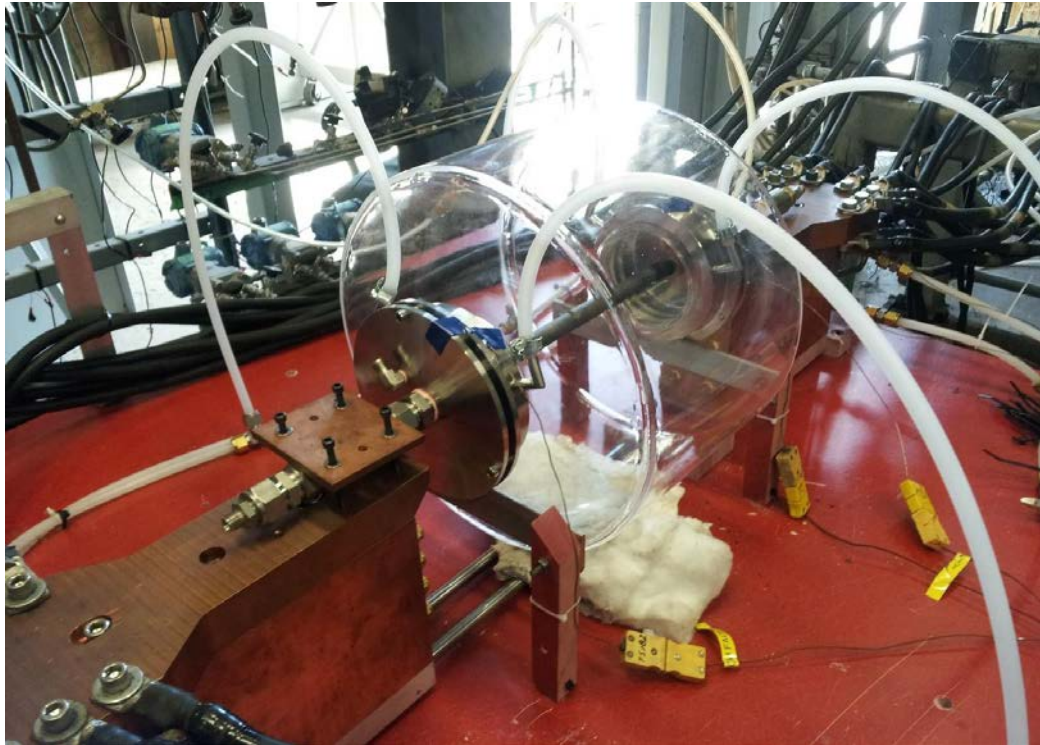


Figure 4-25: HOPE's Test Setup^[57]

Table 4-5: Initial Conditions under Steady State in HOPE's Experiment

Parameter	Value
Atmosphere temperature	300K
Inlet pressure	110kPa
Ambient pressure	10^{-3} Pa
Voltage	150V
Constant capacitance	$1.00054 \mu F$

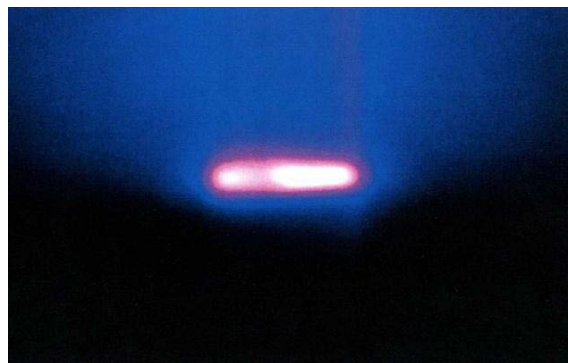


Figure 4-26: High-current Plasma Beams Formed across Two Plasma Jets^[58]

To initiate a plasma, a voltage is applied to both ends of the single carbon tube passing

through the chamber. A notch or a length of thinner tube is made at the center point of the carbon tube. The tube vaporizes starting from the center thinned-down location, and a high-current plasma beam is generated and maintained by the supplied voltage and current, as shown in **Figure 4-26**. When the current passing through the argon gas is high enough, a pinched plasma beam forms under the influence of the Lorentz force. The remaining halves of the tubes continue to act as the electrodes to feed current through plasma beams. The high temperature plasma as well as the current continue to vaporize the ends of the carbon graphite tube and widen the gap until the tube is consumed or until its temperature no longer increases. The plasma beam is extinguished when the gap between the electrodes exceeds the length at which the voltage are needed to maintain high-current plasma beams.

4.4.3 Experimental Results and Analysis

1. Power Supply

- 1) Rippled DC, rectified from 60Hz AC supply with 12 pulses per cycle
- 2) Max 640V adjustable ($\pm 320V$ with center tap connected to ground potential)
- 3) Max 8kA adjustable
- 4) Operation mode: current mode

2. Gas Supply

Argon is initially used to fill the test chamber and subsequently fed into the carbon graphite tube from the negative terminal.

4.4.3.1 Measurement

The voltage, current and temperature are measured in HOPE's experiment as following:

- 1) Voltage should be measured directly between the two electrodes;
- 2) Current is measured using the inductance pickups near the apparatus;
- 3) Thermocouples are placed on the electrodes, quartz chamber and cooling blocks and on any temperature-sensitive components;

- 4) Methods for measuring plasma temperature and cation and electron speed in the plasma are being developed in collaboration with HOPE's R&D partners.

4.4.3.2 Experimental Data

In **Figure 4-27(a)**, we can see that the voltage and current continuously change with the time. The two solid lines denote the polynomial fittings of the voltage and current. The average of voltage and current are approximately 150 V and 335A. In **Figure 4-27(b)**, we can obtain the relationship between the voltage and current and directly read their polynomial equations.

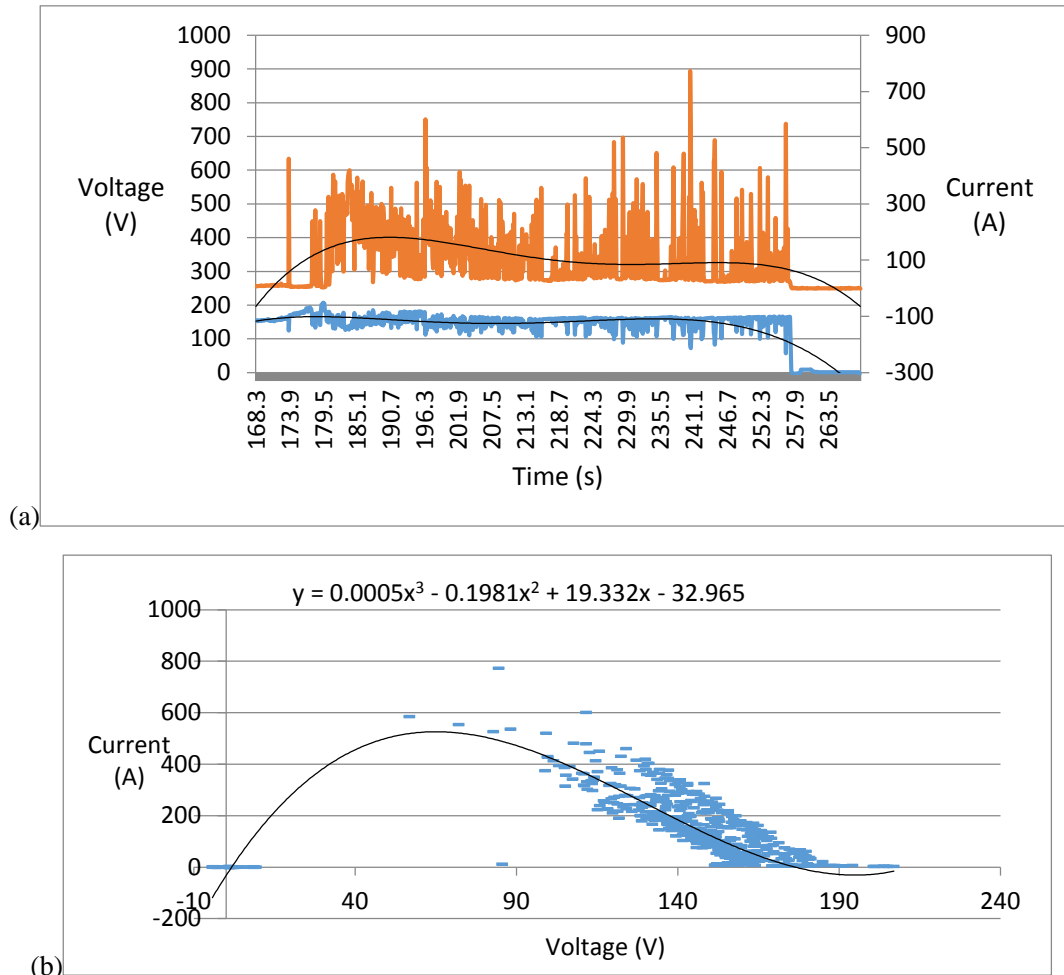


Figure 4-27: (a) Current (Red Line) & Voltage (Blue Line) vs. Time and (b) Polynomial Equation for Voltage vs. Current in HOPE's Experiment

In **Figure 4-28**, in the beginning, the temperature violently changes. With the time goes by, it changes more steadily. During the process, although the power increases, the

temperature does not change irregularly, which is approximately equal to 1500K.

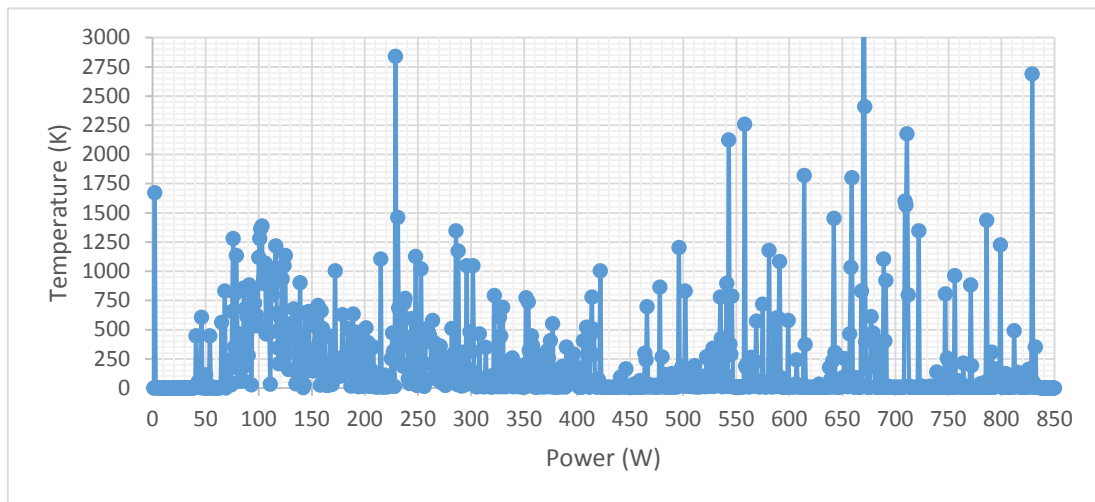


Figure 4-28: Power vs. Temperature in HOPE’s Experiment

4.4.3.3 One-Way Analysis of Variance

From the summary part in **Table 4-6** and **Table 4-7**, we obtain the sum, mean and variance of voltage and current, respectively. From the ANOVA part, in **Table 4-6**, because p is equal to 0.667554, which is larger than 0.05 at the 0.05 level, the mean difference is not significant. Similarly, in **Table 4-7**, because P -value is equal to 0.078316, which is larger than 0.05 at the 0.05 level, the mean difference is not significant. Therefore, the changing time has no significant influence on the voltage and current measurement. This means that the measured values are close to the calculated theoretical values.

We also see that the variance sources come from three parts: variance between groups, variance within groups and variance in total groups.

Table 4-6: Analysis of Variance (ANOVA) Table for Voltage

Summary					
Groups of current	Number	Sum	Mean	Variance	
Group 1	12	1821	151.75	7.295455	
Group 2	12	1816	151.3333	3.69697	
ANOVA					
Difference source	SS	Df	MS	F-ratio	P-value
Between groups	1.041667	1	1.041667	0.189524	0.667554
Within groups	120.9167	22	5.496212		
Total	121.9583	23			

Table 4-7: ANOVA Table for Current

Summary					
Groups of current	Number	Sum	Mean	Variance	
Group 1	12	3945	328.75	381.8409	
Group 2	12	4157	346.4167	716.6288	
ANOVA					
Difference source	SS	Df	MS	F-ratio	P-value
Between groups	1872.667	1	1872.667	3.409592	0.078316
Within groups	12083.17	22	549.2348		
Total	13955.83	23			

where SS denotes sum of squares, Df denotes degree of freedom and MS denotes mean square.

4.4.4 Three Methods Verification

1. Quantitative Plasma Energy

For plasma energy in the MHD simulations using **Equation 3.3** in **Section 3.2.2**, the energy of a plasma equals to the sum of thermal energy, Ohm's heating and radiation.

The energy density, E_d , is the summation of the internal energy, the kinetic energy and the energy of the magnetic field^[59] with the unit J:

$$E_d = \frac{p}{r_h - 1} + \frac{1}{2} \rho \vec{v} \cdot \vec{v} + \frac{\overline{\vec{B} \cdot \vec{B}}}{2\mu_0} \quad (4.7)$$

where the term $\frac{\overline{\vec{B} \cdot \vec{B}}}{2\mu_0}$ denotes the plasma energy of magnetic field, which are assumed to be produced from either plasma by an external magnetic field.

For plasma energy in the MC simulations, the electron flux and deposit energy are used to calculate the plasma energy with the unit 10^9eV . For plasma energy in the HOPE's experiment, power is equivalent to the plasma energy with the unit W. For the IMHDMC method, it combines the MHD and MC simulations so that the sum of them represent plasma energy in the IMHDMC simulations. In **Figure 4-29**, the MHD, MC and HOPE's experiment plasma energy are illustrated, where the X-axis is the length of the plasma beam and the Y-axis is the plasma energy. It is obvious that each of plasma energy increases along the Z-axis over time and the plasma energy from the three simulation methods are consistent with the plasma energy from the HOPE's experiment.

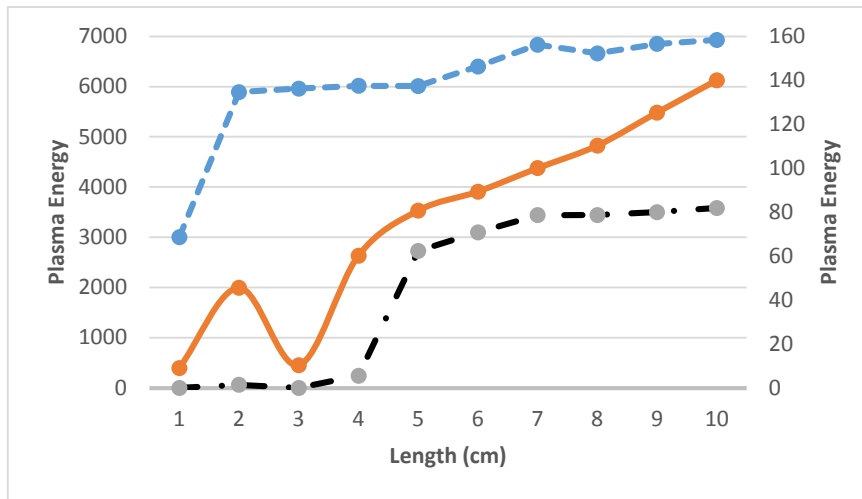


Figure 4-29: HOPE's Experiment (blue line), MHD Simulation (red line) and MC Simulation (black line) for Plasma Energy

2. Qualitative Plasma Dynamics

In the MHD simulation results, the static pressure ($p = \kappa nT$) is not stable and this phenomenon corresponds to the changing temperature in the HOPE's experiment. In the MC simulation results, the amount of particles and heat are the most in the center of the plasma beam. It corresponds to the lightest portion in the center of the plasma beam in

the experiment. In the IMHDMC simulation results, the temperature is the highest in the center of the plasma beam. It corresponds to the highest temperature with the similar value in the experiment. Therefore, the plasma dynamics from the three method simulations have good similarities with the experimental data. To some degree, the three methods are verified in this aspect.

Finally, it is concluded that the three method simulation results are quantitatively and qualitatively consistent with the experimental data.

5 Chapter 5: Comparison, Analysis and Discussion

In **Chapter 5**, we evaluate the MHD, MC and IMHDMC methods. Firstly, in **Section 5.1**, the comparisons between the MHD and MC methods are presented according to the simulation results. In **Section 5.2**, the discussion shows that the three new methods have their own special features and advantages.

5.1 Comparison and Analysis

High-current plasma beams are modeled by the ANSYS FLUENT MHD module. The theory of the MHD module, along with the governing equations in the differential form and boundary conditions, are given. According to the MHD simulation results, the Lorentz force is a main parameter which affects a fluid flow in magnetic fields. In the MC method, the high-current plasma beams are simplified as beams ionized by the e-beam source in the magnetic fields. The MC method includes the particle transport process and collision. According to the MC simulation results, the magnetic fields in the PHITS geometries change the particle trajectories. The heat and deposit energy are increased by the magnetic fields. The similarities and differences between the MHD and MC simulations are listed in **Table 5-1**.

Table 5-1: Similarities and Differences between MHD and MC Simulations

Similarities	<ol style="list-style-type: none"> 1) Same geometry: two cylinders 2) Same materials: argon gas and a copper wall 3) Same parameter values: length and radius
Differences	<ol style="list-style-type: none"> 1) Different states: the steady state for the MHD method and the transient state for the MC method 2) Different initial settings: the initial velocity for the MHD method and the initial projectile energy of electron for the MC method 3) Different evaluation standards: tolerance for the MHD method and relative errors for the MC method 4) Different running time: 10-20minutes per simulation for the MHD method and 30-100 minutes per simulation for the MC method 5) Different control functions: solution control panel for the MHD method; history number, cut-off energy and data libraries function for the MC method

5.2 Discussion

5.2.1 Theoretical Aspect

The MHD, MC and IMHDMC methods are compared in **Table 5-2**. These three new methods are all used to study plasma dynamics. However, none of them is capable of simulating plasma transition from a collisionless regime to collisional regime^[60]. Only the MC method can be used to study electron motion. The MHD method assumes quasi-neutrality and neglects mass of electrons. The IMHDMC method is a comprehensive frontier, which bridges collisional and collisionless transition.

Table 5-2: Comparison between MHD, MC and IMHDMC Methods

	MHD method	MC method	IMHDMC method
Approach	Continuum	Particles	Continuum & Particles
Advantage	Accurate	Easy for complex problems and easy for coding	Easy for coding and the fastest one
Disadvantage	Numerically instability	Crude (with error $\propto 1/\sqrt{N}$)	Too many chemical reactions and particles considered

5.2.2 Simulation Aspect

Firstly, in the MHD simulation results, we obtain the static pressure radial distribution and the radial velocity magnitude at the outlet. We also simulate the 3D velocity vector by the vector function. In the MC simulation results, we use the tallies to describe the electron flux on the XY and XZ planes, and the heat and deposit energy distribution. Finally, using the IMHDMC method, which links the MHD and MC simulations together, we can accomplish more accurate and reasonable simulation results: (a) the density profiles calculated by the MC method and (b) the temperature and Lorentz force distribution calculated by the MHD method.

Secondly, the computation time is important and can be regarded as one of simulation difficulties. The MC method approximately takes five hours, the MHD method takes less than one hour and the IMHDMC method takes three hours. The simulation difficulties can be intentionally adjusted by reducing the mesh quality. Therefore, the computational resource is a critical component for MHD, MC and IMHDMC simulations, especially for the MC simulations. The computer resources will be required for more accurate and extensive simulations.

Thirdly, the models of high-current plasma beams in this thesis are not perfect. Although the MHD, MC and IMHDMC simulations are very useful, some details in the simulations are neglected and assumed. For example: in the MHD simulations, the high-current plasma beams are assumed to be turbulent fluid; in the MC simulations, the electric fields are assumed to be uniform; and in the IMHDMC simulations, metastable argon is neglected. There are several other models that could be used to simulate high-current plasma beams, such as the two-fluid model. Therefore, further corrections would be necessary for more accurate simulations.

6 Chapter 6: Conclusion and Future Work

6.1 Conclusion

Using the MHD, MC and IMHDMC methods, we have reached the state in which the 3D simulations with detailed geometry descriptions for high-current plasma beams are conducted. The MHD, MC, and IMHDMC simulations have helped us achieve a better understanding of dynamics of high-current plasma beams. For example: in industrial applications, the simulations could help us improve plasma torch design and fusion energy generation controlling. However, some improvements could be achieved with a higher computing power and the massive use of parallel computing. Most importantly, the complexity of models that are capable of simultaneously describing different processes, has been a limiting factor for high-current plasma beam simulations.

After we identify the velocity and pressure changes by the MHD method; the electron flux and deposit energy by the MC method; and the density, temperature and Lorentz force distribution by the IMHDMC method, it is so important to provide the ability to implement plasma control applications, such as fusion energy generation cooling. It should be pointed out that the high-current plasma beam simulations performed by the MHD, MC and IMHDMC methods in this thesis display a useful starting point to study more complex problems, such as unsteady MHD flow.

6.2 Potential Applications

6.2.1 Fusion Energy Generation Application

The HOPE's Z-Pinch Experiment is an innovative confinement concept to magnetically confine a high-temperature and high-density plasma. A Z-pinch has a simple and linear configuration with no magnetic field coils: axial plasma current generates azimuthal magnetic fields that confine and compress the plasma. The Z-pinch concept is

investigated in formative years of fusion energy development. Plasma instabilities, such as sausage and kink modes, limit achievable parameters and hinder progress of the Z-pinch concept. However, more recent theoretical investigations have presented a mechanism to stabilize Z-pinch plasmas using a shear flow. In **Figure 6-1**, there is a basic explanation of how a Z-pinch works.

1. Pinches apply a huge voltage across a tube, which is filled with fusion fuel. The gas ionizes when the voltage times charge is higher than ionization energy of a gas.
2. Current jumps across this gap.
3. The current makes magnetic fields which are perpendicular to the current. This magnetic fields try to pull material together.
4. These atoms could draw close enough to fuse.

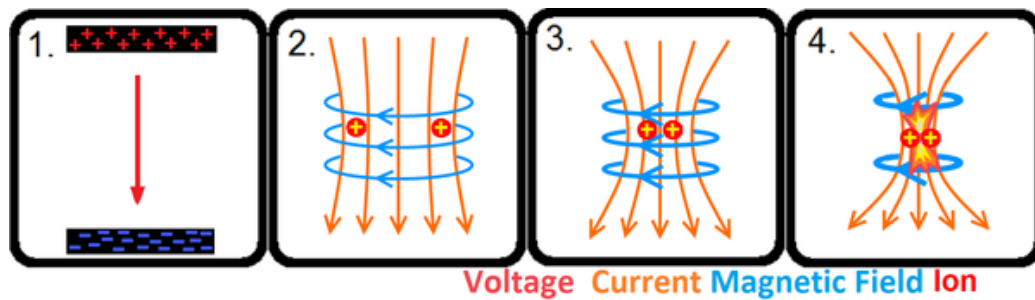


Figure 6-1: Basic Z-pinch Mechanism^[61]

The HOPE has developed an alternative approach to generate fusion energy based on the concept of four high-current plasma beams passing through a common intersection point called the focal region^[62], as shown in **Figure 6-2**. The four high-current plasma beams are symmetrically arranged in 3D space in a tetrahedral configuration. This innovative configuration can improve plasma stability in the focal region.

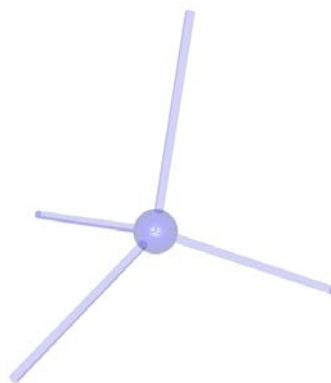


Figure 6-2: Four Intersecting Plasma Beam Model^[63]

6.2.2 Plasma Gasification Application

Plasma gasification is a process which converts organic matter into synthetic gases, electricity and slag by using high-current plasma beams. In **Figure 6-3**, the two plasma arc torches are the main elements and are powered by electric arcs. The plasma gasification is commercially used as a form of waste treatment. A plasma torch uses an inert gas and electrodes vary from copper to tungsten and other alloys. High current are produced by high voltage, which pass between two electrodes to produce a high-current plasma beam (an electric arc). The pressurized inert gas is ionized passing through the plasma beam. When the torch temperature is very high, molecular bonds break down to create basic material atoms.



Figure 6-3: Westinghouse Plasma Gasification. (Westinghouse Plasma Corporation)^[64].

Waste processing by plasma gasification is an ecologic process, as shown in **Figure 6-4**. Due to lack of oxygen and existing high temperature in a waste processing reactor, it prevents main elements of gases from forming toxic compounds, such as NO_x . The filtration systems remove inorganic residue and gaseous pollutants so that they produce clean synthetic gases. At the same time, the circulating water in the filtering systems has removed hazardous substances. Next, the synthetic gases produced by the last step is used for power supply and the gaseous pollutants are converted to valuable chemical

products. Finally, the inert slag is used in construction and the left metal is used for production of alloy.

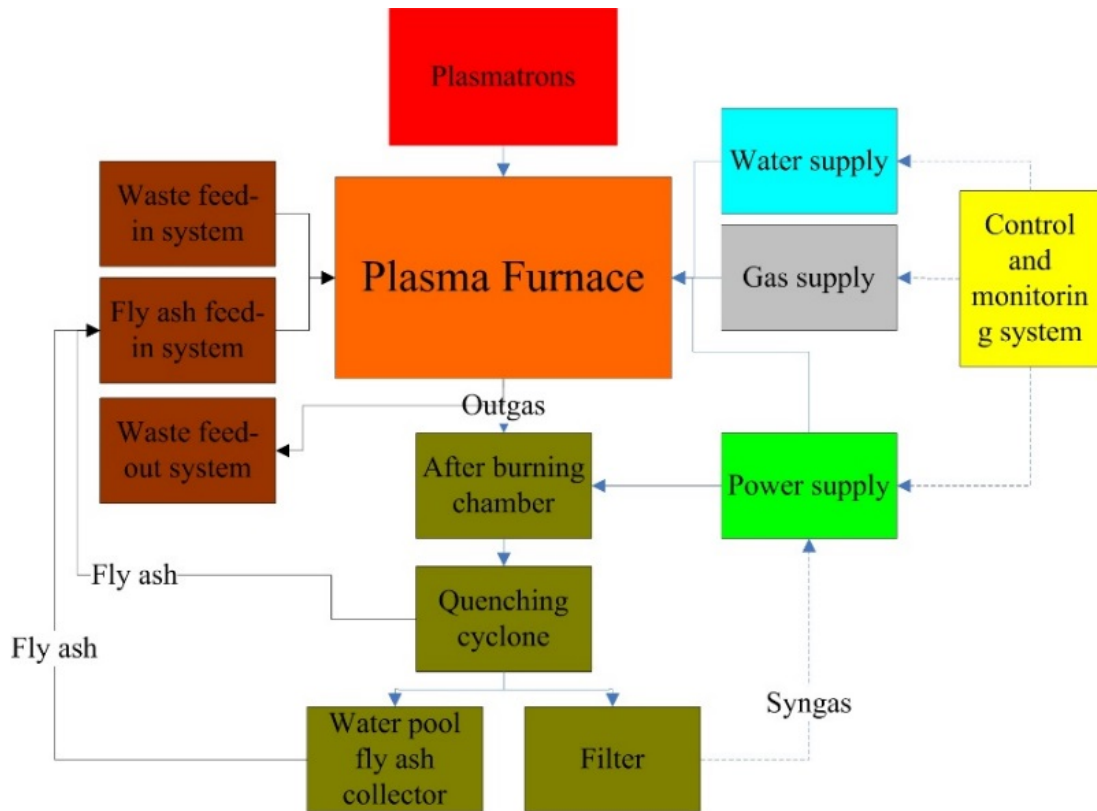


Figure 6-4: Waste Processing by Plasma Gasification

6.3 Future Work

Optimization of the MHD, MC and IMHDMC models of high-current plasma beams in industrial applications, may improve their performance further. A list of prospective optimizing activities may include:

1. The mesh grid quality in the three models could be improved by using a different type of mesh grids since mesh grids are varied in geometry, boundary conditions and material. The improvements could be conducted by iteratively changing size and shape of elements and relative dimensions of neighboring elements.
2. Other pure gases or mixtures could be applied in the three models. After we have a wide range of simulation results, it is easy to choose the most efficient gases or mixtures in industrial applications.

In the future, we will do other useful measurement and development for HOPE's experiment. For example, we could use a Langmuir electrostatic probe to measure electron density and temperature. At the same time, because the magnetic fields in the plasma are periodic, the rate of change of the magnetic field with time can be measured locally by magnetic probe. More intersecting plasma beams would be applied to the MHD, MC and IMHDMC models. The interaction effects can be explored between the two or more plasma beams using the MHD, MC and IMHDMC methods. Besides, prospective activities would involve a separate validation for the IMHDMC method.

Appendices

Appendix A: List of Acronyms

1D/2D/3D	One/ Two/ Three Dimensional
API	Application Programming Interface
ANOVA	Analysis of Variance
CFD	Computational Fluid Dynamics
DC	Direct current
Df	Degree of freedom
e-beam	electron beam
EPS	Encapsulated PostScript
FEM	Finite Element Method
Fortran	Formula Translating System
FVM	Finite Volume Method
GG	General Geometry
HOPE	HOPE Innovations Inc.
ID	Inner Dimension
IMHDMC	Integrated Hybrid MHD and MC Method
k- ϵ	K-epsilon
KERMA	Kinetic Energy Released per unit Mass
LTE	Local Thermodynamic Equilibrium
MCNP	Monte Carlo N-Particle
MHD	Magnetohydrodynamics
MS	Mean square
NEC	Net Emission Coefficient
NMTC	Nuclear Meson Transport Code
OD	Outer Dimension
PDEs	Partial Differential transport Equations

PENELOPE Penetration and ENergy Loss of Positrons and Electrons

PHITS Particle and Heavy Ion Transport code System

PIC Particle-In-Cell

PS PostScript

PTSG Plasma Theory and Simulation Group

RDD Radiological Dispersal Device

SIMPLE Semi-Implicit Method for Pressure-Linked

SS Sum of squares

STL Standard Template Library

Appendix B: Nomenclature

Ar^0 argon atoms

Ar^+ argon ions

B magnetic field

c_s speed of sound in a plasma

C capacitance

C_p specific heat

d distance

e electron charge

e^- electron

E_c cut-off energy

E_d plasma energy density

E_k kinetic energy

F Lorentz force

h specific total enthalpy

I current

J current density

K_n Knudsen number

L number of steps

L_r	representative physical length scale
m	mass
M	Mach number
n	particle density
n_e	electron concentration
N	total number of particles or histories
N_1/N_2	uniform random numbers
p	pressure
q	particle charge
Q	charge stored in a capacitor
r	radius
r_h	heat capacity ratio
S_{rad}	radiation losses
t	time
T	temperature
T_t	total thickness
u, v, w	velocity in x, y, and z direction
w_i/\bar{w}	source weight of each sample/ means values of the source weights
x, y, z	Cartesian coordinate system
x_i/\bar{x}	tally results/ mean values of the tally results
V	voltage across the capacitor
Z	depth
Z-pinch	Zeta pinch

Greek Symbols

μ_0	magnetic permeability
μ_e	electron mobility
ϕ	electric potential
ρ	charge density

κ	Boltzmann constant
ε_0	electric permittivity
ξ	energy
τ	viscous stress
η	electrical resistivity
λ	thermal conductivity
λ_m	mean free path
σ	electrical conductivity
σ_d	standard deviation
θ / φ	polar angle
ω	cyclotron frequency

Subscripts

e	electron
exc	excitation
EAS	EquiAngle Skew
i	ion
ion	ionization
max	maximum
min	minimum
p	particle

Appendix C: Physical Constants

Permittivity of free space	$\varepsilon_0 = 8.8542 \times 10^{-12} F / m$
Permeability of free space	$\mu_0 = 4\pi \times 10^{-7} H / m$
Boltzmann constant	$\kappa = 1.3807 \times 10^{-23} J / K$
Standard pressure (760Torr=1atm)	$P_0 = 1.0133 \times 10^5 Pa$
Absolute zero temperature	$T_0 = -273.15^\circ C$

Elementary charge

$$q = -1.602 \times 10^{-19} \text{C}$$

In plasma physics, we often use electron volts (eV) and $1 \text{eV} \approx 1.1604 \times 10^4 \text{K}$. In SI units we use Tesla (T) and Gauss (G) for magnetic flux densities and $1 \text{G} = 10^{-4} \text{T}$.

References

- [1]Anthony L. Peratt, “Advances in Numerical Modeling of Astrophysical and Space Plasmas”, *Astrophysics and Space Science*, Vol 242 (1-2), pp: 93-163, 1997.
- [2]B. R. Adhikari, R. Khanal, “Introduction to The Plasma State of Matter”, *The Himalayan Physics*, Vol 4 (4), pp:60-64, 2013.
- [3]Francis F. Chen, “Introduction to Plasma Physics and Controlled Fusion (Volume 1: Plasma Physics) (Second edition)”, *Plenum Press*, New York and London, 1929.
- [4]Daniel J. Ellard, Penelope A. Ellard, “The Monte Carlo Method” in *S-Q 1998 Course Book*, pp: 106-113, 1998.
- [5]T. Sato, K. Niita, N. Matsuda, S. Hashimoto, et al., “Particle and Heavy Ion Transport Code System PHITS, Version 2.52”, *Journal of Nuclear Science and Technology*, Vol 50 (9), pp: 913-923, 2013.
- [6]Michael P. Marder, “Condensed Matter Physics”, *John Wiley & Sons, Inc.*, Second edition, 2010.
- [7]Sudeep Bhattacharjee, “Introduction: Theoretical Approach” in *Compact Plasma Focused Ion Beams*, US: Taylor & Francis Group and The CRC Press, 2013.
- [8]Lu B, Xu L, Zhang X, “Three-dimensional MHD simulations of the electromagnetic flowmeter for laminar and turbulent flows”, *Flow Measurement and Instrumentation*, Vol 33, pp: 239–243, 2013.
- [9]A Lebouvier, S A Iwarere, D Ramjugernath, et al., “3D Magnetohydrodynamic Modelling of A Low-Current Plasma Arc Batch Reactor at Very High Pressure in Helium”, *Journal of Physics D: Applied Physics*, Vol 46 (145203), 2013.
- [10]Bycan Ibrahimoglu, Ahmet Cucen, M. Zeki Yilmazoglu, “Numerical Modelling of DC Arc Plasma Torch with MHD Module”, *International Plasma Technologies Congress*, 2014.
- [11]ANSYS FLUENT Magnetohydrodynamics Module Manual, ANSYS Incorporation, 2013.
- [12] WIKIPEDIA The Free Encyclopedia. (2015, June. 1). K-epsilon turbulence model. [Online]. Available: https://en.wikipedia.org/wiki/K-epsilon_turbulence_model

[13]G. Xu, Junling Hu, H. L. Tsai, “Three-dimensional Modelling of The Plasma Arc in Arc Welding”, *Journal of Applied Physics*, Vol 104 (103301), 2008.

[14]E. G. Sheikin, “Monte Carlo Simulation of Non-equilibrium Conductivity Produced by Electron Beam in MHD Flows”, *48th AIAA Aerospace Sciences Meeting Including the New Horizons Forum and Aerospace Exposition January 2010*, Oriando, Florida

[15]Ondrej Sila, Pavel Kubes, Josef Kravarik, et al., “Estimation of amount of scattered neutron at Devices PFZ and GIT-12 by MCNP Simulations”, *Acta Polytechnica*, Vol 53 (2), pp:228-232, 2013.

[16]Fawaz Ali, “On The Integration of Computational Fluid Dynamics (CFD) Simulations with Monte Carlo (MC) Radiation Transport Analysis”, Master Thesis: University of Ontario Institute of Technology, 2009.

[17]Qing Yang, “A Computational Fluid Dynamic Approach and Monte Carlo Simulation of Phantom Mixing Techniques for Quality Control Testing of Gamma Cameras”, Master Thesis: University of Canterbury, 2013.

[18]Impedans Limited Company. (2015, Sept. 25). Langmuir Probe. [Online]. Available: <http://www.impedans.com/langmuir-probe>

[19]WIKIPEDIA The Free Encyclopedia. (2015, June. 16). Knudsen Number. [Online]. Available: https://en.wikipedia.org/wiki/Knudsen_number

[20]Annemie Bogaerts, Renaat Gijbels, “Hybrid Monte Carlo-fluid modeling network for an argon/ hydrogen direct current glow discharge”, *Spectrochimica Acta Part B*, Vol 57, pp: 1071-1099, 2002.

[21]Alexandre lebouvier, Clarisse Delanlondrer, Francois Fresnet, et al., “Three-Dimensional Unsteady MHD Modeling of A Low-Current High-Voltage Nontransferred DC Plasma Torch Operating with Air”, *IEEE Transactions on Plasma Science*, Vol 30 (9), 2011.

[22]He-Ping Li, E. Pfender, “Three Dimensional Modeling of The Plasma Spray Process”, *Journal of Thermal Spray Technology*, Vol 16 (2), 2007.

[23]WIKIPEDIA The Free Encyclopedia. (2015, January. 16). Magnetic Reynolds Number. [Online]. Available: https://en.wikipedia.org/wiki/Magnetic_Reynolds_number

[24]K. C. Hsu, K. Etemadi, E. Pfender, “Study of The Free-Burning High-Intensity Argon Arc”, *Journal of Applied Physics*, Vol 54 (3), pp:1293-1301, 1993.

[25] E. Gedik, H. Kurt, Z. Recebli, “CFD Simulation of Magnetohydrodynamic Flow

- of A Liquid-Metal Galinstan Fluid in Circular Pipes”, *Technology Science Press*, Vol 19(1), pp:23-33, 2013.
- [26]D’Angola A, Colonna G, Gorse C and Capitelli M, “Thermodynamic and transport properties in equilibrium air plasmas in a wide pressure and temperature range”, *The European Physical Journal D*, Vol 46, pp: 129–150, 2008.
- [27]Naghizadeh-Kashani Y, Cressault Y and Gleizes A, “Net emission coefficient of air thermal plasmas”, *Journal of Physics D: Applied Physics*, Vol 35, pp: 2925–2934, 2002.
- [28]A. B. Murphy and C. J. Arundell, “Transport coefficients of argon, nitrogen, oxygen, argon nitrogen and argon-oxygen plasmas”, *Plasma Chemistry and Plasma Processing*, Vol 14, pp: 451- 490, 1994.
- [29]J. P. Trelles, C. Chazelas, A. Vardelle, et al., “Arc Plasma Torch Modelling”, Cornell University Library. [Online]. Available: <http://arxiv.org/ftp/arxiv/papers/1301/1301.0650.pdf>
- [30]White WB, Johnson SM and Dantzig GB, “Chemical Equilibrium in Complex Mixtures”, Santa Monica, CA: RAND Corporation, 1957.
- [31]Menart J, Heberlein J and Pfender E, “Line-by-line method of calculating emission coefficients for thermal plasmas consisting of monatomic species”, *Journal of Quantitative Spectroscopy and Radiative Transfer*, Vol 56, pp: 377–98, 1996.
- [32]Evans D L and Tankin R S, “Measurement of emission and absorption of radiation by an argon plasma”, *Physics of Fluids*, Vol 10, pp: 1137–1144, 1967.
- [33]S.G Jennings, “The Mean Free Path in Air”, *Journal of Aerosol Science*, Vol 19 (2), pp: 159-166, 1988.
- [34]Ryuichi Shimizu and Ding Ze-Jun, “Monte Carlo modelling of electron-solid interactions”, *Progress Physics*, pp:487-531, 1992
- [35]Multi-Purpose Particle and Heavy Ion transport code System, “PHITS Basic Lecture II: Definitions of Tally”, 2015.
- [36]Katsuhisa Koura, “Null-Collision Technique in The Direct-Simulation Monte Carlo Method”, *Physics of Fluids*, Vol 29 (11), pp: 3509-3511, 1986.
- [37]H. R. Skullerud, “The stochastic computer simulation of ion motion in a gas subjected to a constant electric field”, *Journal of Physics D: Applied Physics*, Vol 1(11): 1597, 1968.

- [38]R. Razdan, C. E. Capjack, and H. J. J. Seguin, “Influence of a magnetic field on the growth of instabilities in a helium glow discharge using Monte Carlo simulation of the cathode fall region”, *Journal of Applied Physics*, Vol 57: 4954, 1985.
- [39]R. Razdan, C. E. Capjack, and H. J. J. Seguin, “Monte Carlo simulation of the cathode fall region of a CO₂ laser glow discharge for studying the influence of magnetic fields on instability growth”, *Applied Optics*, Vol 25 (17), pp: 2915-2925, 1986.
- [40]Hossam A. Gabber, Luping Zhang, Emmanuel Boafo et al., “3D Time-Dependent Simulation of High-Current Plasma Beam Model by Magnetohydrodynamics and Monte Carlo Methods”, *Plasma Science Technology*, Paper submitted, 2015.
- [41]Jun Li, Qing-Ming Chen, Zai-Guang Li, “Monte Carlo Simulation of Electron Motion in The Cathode Region of A Magnetron Glow Discharge in Argon”, *Journal of Physics D: Applied Physics*, Vol 28, pp:681-688, 1994.
- [42]Dai Sheng Mao and Qing Ming Chen, “Monte Carlo simulation of electron motion in magnetically confined CO gas laser discharges”, *Journal of Physics D: Applied Physics*, Vol 28, pp:1111-1120, 1995.
- [43]A.V. Phelps. (2015, Sept. 25). PHELPS database. [Online]. Available: http://fr.lxcat.net/data/set_type.php
- [44]Annemie Bogaerts, Erik Neyts, Renaat Gijbels, et al., “Gas Discharge Plasmas and Their Applications”, *Spectrochimica Acta Part B*, Vol 57, pp: 609-658, 2002.
- [45]Annemie Bogaerts, “Hybrid Monte Carlo-Fluid Modelling Network for An Argon/Hydrogen Direct Current Glow Discharge”, *Spectrochimica Acta Part B*, Vol 57, pp: 1071-1099, 2002.
- [46] ANSYS FLUENT 12.0 User’s Guide. (2009). ANSYS Incorporation. [Online]. Available: <http://users.ugent.be/~mvbelleg/flug-12-0.pdf>
- [47]WIKIPEDIA The Free Encyclopedia. (2015, August. 21). Mach number. [Online]. Available: https://en.wikipedia.org/wiki/Mach_number
- [48]Masoud Yousef Ramandi, “Muti-Dimensional Modeling of Transient Transport Phenomena in Molten Carbonate Fuel Cells”, PHD Dissertation, University of Ontario Institute of Technology, 2012.
- [49]ANSYS Inc., “Pressure-based Solver” in FLUENT 6.3 Documentation. [Online]. Available: <https://www.sharcnet.ca/Software/Fluent6/html/ug/node987.htm>

- [50]Bo Lu, Liangwang Xu, Xiaozhang Zhang, “Three-Dimensional MHD Simulations of The Electromagnetic Flowmeter for Laminar and Turbulent Flows”, *Flow Measurement and Instrumentation*, Vol 33, pp: 239-243, 2013.
- [51]E. Eylenceoglu, I. Rafatov, and A. A. Kudryavtsev, “Two-dimensional hybrid Monte Carlo-fluid modelling of dc glow discharges: Comparison with fluid models, reliability, and accuracy ”, *Physics of Plasmas*, Vol 22: 013509, 2015.
- [52]H. Iwase, K. Niita, T. Nakamura, “ Development of general-purpose particle and heavy ion transport Monte Carlo code ”, *Journal Nuclear Science and Technology*, Vol 39 (1142), 2002.
- [53]K. Niita, T. Sato, H. Iwase, H. Nose, H. Nakashima, L. Sihver, “ PHITS-a particle and heavy ion transport code system ”, *Radiation Measurements*, Vol 41 (1080), 2006.
- [54]K. Niita, et al. “High Energy Particle Transport Code NMTC/JAM”, JAERI-Data/Code 2001-007, Japan Atomic Energy Research Institute, 2001.
- [55]A Derzsi, P Hartmann, I Korolov, et al., “On The Accuracy and Limitations of Fluid Models of The Cathode Region of DC Glow Discharge”, *Journal of Physics D: Applied Physics*, Vol 42 (22), 2009.
- [56]WIKIPEDIA The Free Encyclopedia, Capacitance, (2015, Sept.5). [Online]. Available: <https://en.wikipedia.org/wiki/Capacitance>
- [57]W. Liu, A. Wallace, “Single Plasma Beam Experiment Test Plan”, HOPE Document No. SL14-01-WP-001-R00-CONF from HOPE Innovations Inc., 2014.
- [58]B. O. Deng, Z. X. Gan, J. J. Gu, et al., “Fusion Power Based on A Symmetrical Plasma Beam Configuration”, A scientific paper to be submitted for publication, 2014.
- [59]Clyde Albert Jr. Barry Stoute, “Hybrid Electric Thruster Using Gas Mixtures”, PHD Dissertation, York University, 2013.
- [60]S. A. Ledvina, Y. J. Ma et al., “Modeling and Simulating Flowing Plasmas and Related Phenomena”, *Space Science*, 2008.
- [61]Wikipedia, the free encyclopedia. (2015, Sept. 10). Pinch (Plasma Physics). [Online]. Available: [https://en.wikipedia.org/wiki/Pinch_\(plasma_physics\)](https://en.wikipedia.org/wiki/Pinch_(plasma_physics))
- [62]F. Miao, X. J. Zheng, and B. Q. Deng, “Fusion of Multi-pinched Plasma Beam Converging with Spatial Symmetry”, *Plasma Science and Technology*, 2015.
- [63]B. Q. Deng, Z. X. Gan, J. J. Gu, et al., “Fusion Power Based on A Symmetrical Plasma beam Configuration”, A scientific paper to be submitted for publication, 2014

[64]Westinghouse Electric Corporation and Westinghouse Plasma Corporation. (2015, Sept.25). Waste to Energy. [Online]. Available: http://www.westinghouse-plasma.com/waste_to_energy/